NAVAL POSTGRADUATE SCHOOL

MONTEREY, CALIFORNIA

THESIS

GEANT4 SIMULATION OF FAST NEUTRON INTERACTIONS IN HEAVY OXIDE SCINTILLATORS

by

Bruce Batteson

September 2019

Thesis Advisor:	Craig F. Smith
Second Reader:	Dragoslav Grbovic

THIS PAGE INTENTIONALLY LEFT BLANK

REPORT DOCUMENTATION PAGE	*Form Approved OMB No. 0704-0188*

1. AGENCY USE ONLY *(Leave blank)*	**2. REPORT DATE** September 2019	**3. REPORT TYPE AND DATES COVERED** Master's thesis

4. TITLE AND SUBTITLE GEANT4 SIMULATION OF FAST NEUTRON INTERACTIONS IN HEAVY OXIDE SCINTILLATORS	**5. FUNDING NUMBERS** RPMGJ
6. AUTHOR(S) Bruce Batteson	
7. PERFORMING ORGANIZATION NAME(S) AND ADDRESS(ES) Naval Postgraduate School Monterey, CA 93943-5000	**8. PERFORMING ORGANIZATION REPORT NUMBER**
9. SPONSORING / MONITORING AGENCY NAME(S) AND ADDRESS(ES) RD-NT (NSERC), DTRA, West Point, NY	**10. SPONSORING / MONITORING AGENCY REPORT NUMBER**

11. SUPPLEMENTARY NOTES The views expressed in this thesis are those of the author and do not reflect the official policy or position of the Department of Defense or the U.S. Government.

12a. DISTRIBUTION / AVAILABILITY STATEMENT Approved for public release. Distribution is unlimited.	**12b. DISTRIBUTION CODE** A

13. ABSTRACT (maximum 200 words)

Fast neutron detection is critical to the interdiction of illicit special nuclear material, among other potential applications. The use of heavy oxide scintillators to detect fast neutrons is one technology requiring little to no moderation and enabling construction of highly efficient detectors. Previous work qualitatively describes various physical modes of neutron interaction in these materials. This work simulates the interaction of neutrons in heavy oxide materials in order to quantify the contribution of each physical mode to the overall detection signal and to evaluate the chain of reactions from incident neutron to optical photon production and transport. Such quantization may enable optimization of detector design and greater fidelity in detector response.

Using GEANT4 in conjunction with Lawrence Livermore National Laboratory's LEND physics list, we simulated the response of Bismuth Germanate ($Bi_4Ge_3O1_2$ or BGO) to incident neutrons. We validated the simulation by comparison to known data and laboratory experimental results. Optical photon production was generally a result of complex and highly varied series of particle interactions. Although we identified hundreds of unique photon production channels in BGO, relatively few such channels played a significant role in optical photon production. We observed that 90% of photon production was through a channel that started with an initial neutron elastic or inelastic scattering event.

14. SUBJECT TERMS fast neutron detection, inelastic neutron scattering, resonant neutron capture, heavy oxide scintillator, bismuth germanate, $Bi_4Ge_3O1_2$, BGO, GEANT4 simulation toolkit, G4OpticalPhysics, LEND.	**15. NUMBER OF PAGES** 75
	16. PRICE CODE

17. SECURITY CLASSIFICATION OF REPORT	**18. SECURITY CLASSIFICATION OF THIS PAGE**	**19. SECURITY CLASSIFICATION OF ABSTRACT**	**20. LIMITATION OF ABSTRACT**
Unclassified	Unclassified	Unclassified	UU

NSN 7540-01-280-5500

Standard Form 298 (Rev. 2-89)
Prescribed by ANSI Std. 239-18

THIS PAGE INTENTIONALLY LEFT BLANK

Approved for public release. Distribution is unlimited.

GEANT4 SIMULATION OF FAST NEUTRON INTERACTIONS IN HEAVY OXIDE SCINTILLATORS

Bruce Batteson
Lieutenant Commander, United States Navy
BS, Pennsylvania State University, 2006

Submitted in partial fulfillment of the
requirements for the degree of

MASTER OF SCIENCE IN PHYSICS

from the

NAVAL POSTGRADUATE SCHOOL
September 2019

Approved by: Craig F. Smith
Advisor

Dragoslav Grbovic
Second Reader

Kevin B. Smith
Chair, Department of Physics

THIS PAGE INTENTIONALLY LEFT BLANK

ABSTRACT

Fast neutron detection is critical to the interdiction of illicit special nuclear material, among other potential applications. The use of heavy oxide scintillators to detect fast neutrons is one technology requiring little to no moderation and enabling construction of highly efficient detectors. Previous work qualitatively describes various physical modes of neutron interaction in these materials. This work simulates the interaction of neutrons in heavy oxide materials in order to quantify the contribution of each physical mode to the overall detection signal and to evaluate the chain of reactions from incident neutron to optical photon production and transport. Such quantization may enable optimization of detector design and greater fidelity in detector response.

Using GEANT4 in conjunction with Lawrence Livermore National Laboratory's LEND physics list, we simulated the response of Bismuth Germanate ($Bi_4Ge_3O1_2$ or BGO) to incident neutrons. We validated the simulation by comparison to known data and laboratory experimental results. Optical photon production was generally a result of complex and highly varied series of particle interactions. Although we identified hundreds of unique photon production channels in BGO, relatively few such channels played a significant role in optical photon production. We observed that 90% of photon production was through a channel that started with an initial neutron elastic or inelastic scattering event.

THIS PAGE INTENTIONALLY LEFT BLANK

TABLE OF CONTENTS

LIST OF FIGURES

LIST OF TABLES

THIS PAGE INTENTIONALLY LEFT BLANK

LIST OF ACRONYMS AND ABBREVIATIONS

BGO	bismuth germanate ($Bi_4Ge_3O_{12}$)
CERN	Conseil Européen pour la Recherche Nucléaire (the European Organization for Nuclear Research)
eV	electron volt
ENDF	evaluated nuclear data file
G4NDL4.5	GEANT4 nuclear data library, version 4.5
GEANT4	geometry and tracking, version 4
GND	generalized nuclear data
GSO	gadolinium orthosilicate (Gd_2SiO_5Ce)
JENDL	Japanese evaluated nuclear data library
LEND	low energy nuclear data
LLNL	Lawrence Livermore National Laboratory
LUT	lookup table
MCNP6	Monte Carlo N-Particle, version 6
MeV	megaelectron volt
NPS	neutrons per second
NXSG4	an extension to GEANT4 developed by Kittelmann and Boin at the European Spallation Source
PMT	photomultiplier tube
ROOT	an object-oriented data analysis framework developed at CERN
SNM	special nuclear material
ZWO	zinc tungstate ($ZnWO_4$)

THIS PAGE INTENTIONALLY LEFT BLANK

ACKNOWLEDGMENTS

This work was made possible in collaboration with Lawrence Livermore National Laboratory and with the financial support of the Defense Threat Reduction Agency Nuclear Science and Engineering Research Center.

I would like to express my deepest appreciation to my Naval Postgraduate School advisor, Professor Craig Smith, for his guidance and teaching. His vision, discussions on physics, and grounding in the applications of this project were essential to its success.

I am indebted to Dr. Jerome Verbeke and Dr. Phil Kerr at Lawrence Livermore National Laboratory for their collaboration in this work. Jerome's patient tutoring on the intricacies of GEANT4 and his common sense approach to interpreting the simulation results were crucial to developing a working model. The experimental portion of this work would not have been possible without Phil. Phil's technical knowledge and laboratory expertise were critical in the design and execution of the experiments used to test our simulation results.

I am deeply grateful to my family for their support of this work. I thank my parents for instilling in me discipline and a lifelong love of learning. Above all, I cannot imagine accomplishing this work without the tireless support of my loving wife, Alicia, and the contagious energy and endless inspiration of my two boys, Michael and Alex.

THIS PAGE INTENTIONALLY LEFT BLANK

I. INTRODUCTION

A. BACKGROUND

Fast neutron detection is critical to the interdiction of illicit special nuclear material (SNM). Currently fielded ^{3}He detectors typically rely on moderating material such as polyethylene or other hydrogenous material to slow incident neutrons to thermal levels where they can interact with ^{3}He and thus be registered in the detector. However, such moderation substantially increases the size of the detector and limits the efficiency of detection.

The low efficiency of current ^{3}He-based detectors against fast neutron sources combined with shortages of raw ^{3}He have spurred recent work in alternative detector technologies. Many avenues are being pursued, but one of the most promising is the use of heavy oxide scintillators, such as bismuth germanate ($Bi_4Ge_3O_{12}$ or BGO), gadolinium orthosilicate (Gd_2SiO_5Ce or GSO) and zinc tungstate ($ZnWO_4$ or ZWO) to detect fast neutrons [1]. This method requires little to no moderation and enables construction of highly efficient, compact (man-portable), and rugged detectors.

Previous work has demonstrated the potential of heavy oxide scintillators as a suitable material for detection of fast neutrons, in particular to enable interdiction of illicit SNM. Experiments have demonstrated fast neutron detection efficiencies near 50% for single crystal detectors as well as ZEBRA detectors (multilayer detectors with composite heavy oxide scintillators as in the sample shown in Figure 1) based on BGO, GSO, or ZWO [2].

The ultimate detection signal of a scintillation detector is based on the counting of optical photons by a photodetection device such as a photomultiplier tube (PMT). Scintillator detectors consist of a wide variety of substances, and their responses to various types of radiation can vary greatly. A review of the evaluated nuclear data file (ENDF) reveals many possible neutron interaction channels in heavy oxide scintillators [3]. Ryzhikov et al. surmise that elastic scattering, inelastic scattering, and resonant and thermal capture of neutrons are responsible for the detectable signal from heavy oxide scintillators

[1]. Although none of these reactions directly produce detectable optical photons, they start chains of reactions that do. By identifying and quantifying these reaction chains, we hope to provide a basis for better understanding of the processes occurring and thus for optimizing detector design to improve detection efficiency and increase fidelity in interpretation of detector response.

ZEBRA scintillators are proprietary multilayered detectors developed by Ryzhikov et al. at the Institute for Scintillation Materials in Ukraine [4]. ZEBRA scintillators consist of layers of crushed heavy oxide scintillators (such as BGO) embedded in an organic matrix. These composite layers are alternated with layers of clear plastic such as poly(methyl methacrylate) acting as both light guides and as a moderator for incident neutrons.

Figure 1. BGO-based ZEBRA scintillator (left) and BGO monolithic crystal (right)

In this work, conducted in collaboration with Dr. Jerome Verbeke at Lawrence Livermore National Laboratory (LLNL), we are using the GEANT4 simulation toolkit to simulate response of heavy oxide scintillator materials to incident neutrons such as those produced by SNM. GEANT4 is a toolkit originated at CERN (the European Organization for Nuclear Research, or Conseil Européen pour la Recherche Nucléaire) and developed through a worldwide collaboration. It is used to simulate the physics processes of particles passing through and interacting with matter [5]. Data is collected and analyzed using ROOT, a toolkit created at CERN for storage and statistical analysis of large amounts of data [6].

B. RESEARCH OBJECTIVES

This thesis quantifies the reaction channels from incident neutron to photon detection in order to deepen our understanding of these processes and ultimately optimize detector design. This work is intended to provide the foundation for future work in simulation and optimization of neutron detection using heavy oxide scintillators. There are three research objectives:

1. Evaluate the physics lists available in GEANT4 and determine their suitability for this application

2. Quantify the various neutron interaction channels in a particular heavy oxide inorganic scintillator, BGO

3. Evaluate the chain of reactions from incident neutron to optical photon production and transport

C. SCOPE

We chose BGO as the subject of our investigation both due to the potential for the high efficiency direct detection of fast neutrons as identified by Ryzhikov et al. [2], and due to the availability of samples for laboratory testing. Although our work is limited to single crystal BGO scintillators, the methods can readily be extended to other scintillating materials with minor changes to the simulation model.

In the simulation, we consider only the reactions within the scintillator material itself and transport of the optical photons to the face of the photon detector. In practice, the photon detector is typically a PMT. The various PMTs available are well characterized, and it is unnecessary to attempt to reconstruct their design and operation in the simulation. For our purposes, a photon is considered “detected” when it reaches the face of the photon detector.

D. OVERVIEW

This thesis is divided into five chapters: Introduction, Theoretical Considerations, Simulation Construct, Simulation Results, and Conclusion. In the theoretical

considerations we present the physical processes that are necessary to understand the neutron interactions and photon processes implemented in the simulation. The simulation construct outlines the design of our simulation and the methods used to collect simulation data. Simulation results presents the results and analysis. Finally, the conclusion discusses the implications of these results and contains recommendations for future research.

II. THEORETICAL CONSIDERATIONS

The reactions of greatest concern for fast neutron detection are the interactions of incident neutrons with the BGO detector, and the subsequent mechanisms for photon production. A brief review of the ENDF for ^{209}Bi reveals many potential neutron interactions [3]. Considering SNM, we are primarily interested in incident neutrons with energies below 20 MeV. In this energy range, the reactions with generally higher cross sections are elastic and inelastic scattering, neutron capture, and *(n,2n)* reactions.

Being neutral particles, neutrons do not directly produce a scintillation response in the scintillation material. Instead, the interaction of neutrons within the detector causes a variety of processes to occur with corresponding impacts (e.g., recoil, ionization, nuclear excitation) that ultimately trigger the production of scintillation photons within the detector. Some of these reactions produce free electrons that can produce Cerenkov photons contributing to the detection signal.

A. NEUTRON INTERACTIONS

Ryzhikov et al. postulate that the neutron interaction modes with the greatest impact on detector performance are elastic and inelastic scattering and resonant and thermal capture, and that other interactions, such as *(n,2n)*, have a much lesser contribution [1]. Our simulations confirm the significance of elastic and inelastic scattering, but we also observed that the contribution of other reactions such as capture and *(n,α)* depends on the incident neutron energy spectrum.

1. Elastic Scattering

Elastic scattering of neutrons in ^{209}Bi is a significant mode for energies below 1 MeV. Since the energy transfer in elastic scattering is inversely proportional to the atomic number of the target nucleus, elastic scattering is not a significant precursor to optical photon production in ^{209}Bi. However, in BGO, elastic scattering with the ^{16}O nuclei produces gamma quanta when the ^{16}O nuclei de-excite, as shown in Equation (1).

$$A + n \rightarrow A^{*} + n' \rightarrow A + n' + \gamma \quad (1)$$

2. Inelastic Scattering

Inelastic scattering in ^{209}Bi is a significant mode of interaction for neutrons with energies above 1 MeV. At these energies, the neutron and target nucleus form an excited compound nucleus that de-excites emitting prompt gamma quanta. The compound nucleus then decays, emitting the scattered neutron and finally the resulting nucleus de-excites emitting additional gamma quanta [1] as in Equation (2).

$$A + n \rightarrow (A+1)^* \rightarrow (A+1) + \gamma_1 \rightarrow A^* + n' \rightarrow A + n' + \gamma_2 \quad (2)$$

The neutron energy loss and subsequent gamma energy release tend to be much greater for inelastic scattering than for elastic scattering.

3. Neutron Capture

Resonant neutron capture is a significant mode of interaction for neutrons with energies below 1 MeV. Capture occurs when the incident neutron energy matches an excited state of the compound nucleus as in Equation (3). The excited state then decays, producing gamma quanta.

$$A + n \rightarrow (A+1)^* \rightarrow (A+1) + \gamma \quad (3)$$

Thermal neutron capture occurs when incident neutron energy approaches the energies corresponding to ambient temperatures (around 0.025 eV). Although thermal neutron capture has a significantly higher cross section than inelastic scattering, the low levels of thermal neutrons in the unmoderated spectra of neutrons from SNM limit the number of such interactions that are expected to result.

4. *(n,2n)* Reactions

The *(n,2n)* reaction is a significant mode of interaction for energies above 10 MeV. Although this reaction does not directly result in a detectable signal, it increases the number of neutrons available for subsequent reactions.

5. Other Reactions

There are a number of other possible neutron interactions such as proton, deuteron, triton, and alpha production that can also ultimately result in optical photons. However, these reactions contribute significantly less to the detectable signal due to their small cross sections.

B. PHOTON PRODUCTION

1. Scintillation

A scintillating material emits light when exposed to sufficiently energetic radiation. In inorganic crystals such as BGO, this emission is primarily due to excitation and subsequent de-excitation of electrons in the crystal lattice. Within the scintillating material, electrons are permitted in the set of energy bands governed by quantum mechanics. The valence band is the highest filled energy band, and the conduction band is the lowest unfilled band. The energy difference between these two bands is referred to as the band gap (E_g). Incident radiation of sufficient energy to excite an electron from the valence band to the conduction band is considered ionizing radiation. This excitation produces an electron-hole pair. When the excited electron de-excites and recombines with the hole in the valence band, a photon is emitted. This photon emission is called luminescence or scintillation [7].

In practice, the process is more complicated as the crystal structure contains imperfections. The imperfections may be either lattice defects or impurities. Impurities may be incorporated by design to improve scintillation characteristics. In this case, the scintillator is referred to as "activated," as in thallium-activated sodium iodide (NaI-Tl). The imperfections may also simply be an unavoidable result of the manufacturing process. In either case, they result in allowed energy levels between the valence and conduction bands as shown in Figure 2. These energy levels are called centers and can be categorized in three groups: luminescence centers, quenching centers, and traps [7]. Electrons in the conduction band may now occupy one of these centers instead of de-exciting to the valence band.

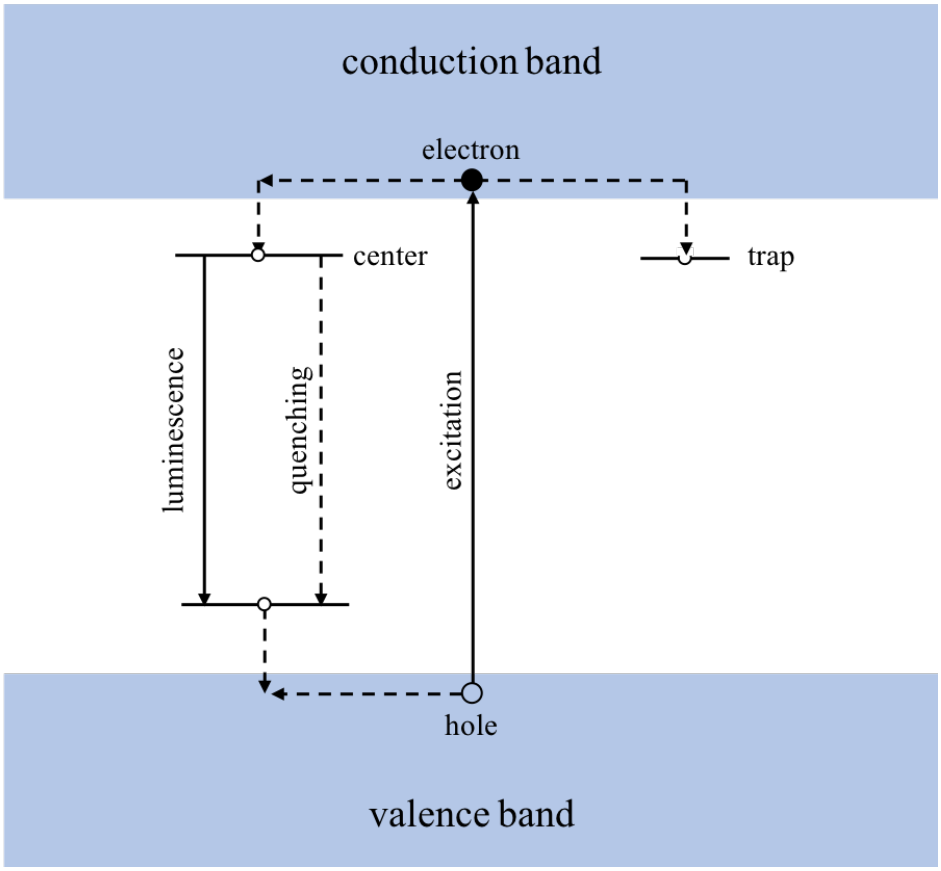

Figure 2. Energy bands in a crystal scintillator. Adapted from [7].

Electrons in luminescence centers will de-excite, emitting a photon, as in the case of the pure crystal. However, in quenching centers, electrons de-excite through emission of phonons, and no photon is emitted. Electrons in traps may either transition back to the conduction band by absorbing a phonon or decay to the valence band by emission of phonons. Thus, the presence of quenching centers and traps reduces the scintillation signal.

The presence of both traps and luminescence centers results in both a fast and slow component of the scintillation signal. Electrons that are excited by the incident radiation and subsequently de-excite through the luminescence center result in prompt photon emission. In contrast, excited electrons may occupy a trap for some period of time before de-exciting through a luminescence center and emitting an optical photon. In BGO, the fast component is emitted in 93.8 ns and the slow component in 368.8 ns [8].

2. Cerenkov Radiation

Cerenkov radiation is the emission of optical photons occurring when a charged particle moves through a dielectric medium with a velocity greater than the local speed of light [9]. The charged particle causes a local polarization of the dielectric as it moves through the material. The subsequent relaxation of this polarization results in the emission of photons. In the case where the charged particle has a velocity less than the local speed of light, it can be shown that the emitted photons destructively interfere [10]. However, if the charged particle has a velocity greater than the speed of light, the photons constructively interfere and we observe a pulse of light. This process is analogous to the bow wave created by a ship moving faster than the wave speed [10].

Although in the particular case of neutron radiation, we are explicitly not considering radiation by charged particles, we do anticipate that both electrons and protons may result from the incident neutrons and subsequent interactions. Taking the index of refraction (n) of BGO to be 2.15 (the actual value varies with wavelength from 2.06 to 2.41 [11]) and using

$$T = \frac{1}{2} m v^2 = \frac{m c^2}{2 n^2}, \tag{4}$$

where T is kinetic energy and we have made use of the fact that $v=c/n$, we find that the minimum energy for an electron to result in Cerenkov radiation is 5.46 keV. It is feasible that electrons will occur with energies above this threshold and so we expect that Cerenkov radiation by electrons may occur in our detector. Similarly, for a proton the threshold energy for Cerenkov radiation in BGO is 100 MeV. Given that we are primarily interested in neutron radiation at levels well below 20 MeV, we do not expect to see Cerenkov radiation by protons in our simulation.

C. CONCLUSION

Many reactions are possible in BGO exposed to neutron radiation. The reactions of greatest interest to this thesis are the initial neutron reactions and the subsequent production of optical photons through scintillation or Cerenkov radiation. Our simulation is designed to capture and analyze the complex relationships of these interactions.

THIS PAGE INTENTIONALLY LEFT BLANK

III. SIMULATION CONSTRUCT

GEANT4 is a powerful simulation toolkit but it requires a significant understanding of C++ object-oriented programming in order to develop a complex simulation. This chapter provides some background on the concept of GEANT4 and the implementation of physics processes and optical photons in the simulation. We present three limitations of our simulation, and finally briefly discuss how data is collected for later analysis.

A. CONCEPT OF GEANT4

GEANT4 stands for GEometry ANd Tracking version 4 and is currently in version 4.10.5. It is an open-source object-oriented program written in C++ by a worldwide collaboration led by CERN. Fundamentally GEANT4 simulates the passage of particles through space and matter using a particular set of physics models specified by the user. The available physics processes include hadronic, electromagnetic, and optical processes [12]. In many cases there is more than one model for a particular physics process and the user can specify which model to apply for a given particle type and energy range.

1. GEANT4 vs. MCMP

Although GEANT4 uses a Monte Carlo method for selecting a given reaction from a particular model, GEANT4 is distinct from Monte Carlo n-particle transport code (MCNP). MCNP is a proprietary, export-controlled software package developed at Los Alamos National Laboratory. Originally intended to model neutron radiation, the current version MCNP6 has developed into a general-purpose radiation model capable of simulating transport of 37 different particle types [13]. Of interest to this work, MCNP6 does not simulate Cerenkov production of photons and implementation of optical photon absorption and scattering is incomplete [10].

2. Physics Lists

Often in physics there exist several unique mathematical models to explain a particular process. The choice of which model to apply in a given scenario typically depends on parameters such as energy or time scale of interest and it is up to the physicist

to select the model that will yield the best result. This is also true in GEANT4 and, as such, it is incumbent upon the user to select which models to apply by carefully crafting the physics list. GEANT4 comes with several prepackaged physics lists called reference physics lists. The user can also create their own custom physics list by specifying the model and cross section data to be applied for a given particle and energy range.

a. Neutron Models

For neutron processes at energies between 5 eV and 20 MeV, there are two models that can be used: The high precision neutron model (NeutronHP) and the low energy nuclear data model (LEND). Both models rely on experimental cross section data and use a Monte Carlo method to select the appropriate reaction.

By default, NeutronHP uses the GEANT4 nuclear data library (G4NDL4.5) data library derived in large part from the ENDF/B-VIII library, but also containing some data from the Japanese evaluated nuclear data library (JENDL). According to the GEANT4 Book for Application Developers [9], there are some peculiarities in a simulation using NeutronHP due to the data available in the ENDF library. While neutron transport and neutron production are reliable, production of charged particles and gamma rays may be less so. In particular, the data libraries do not typically include information on the number and energy of gamma rays produced. In this case GEANT4 applies a simple model that may not accurately reproduce the spectra of gamma rays [9].

LEND uses the generalized nuclear data (GND1.3) library, which derives its data solely from ENDF/B-VIII. The GND1.3 data library includes neutron cross section data for targets from H to Es [15]. In contrast to NeutronHP, LEND is exclusively data-driven so, in the case of gamma ray production, LEND will only produce those gamma rays specified in the data library [16]. As such, LEND may produce more accurate results than NeutronHP, provided that the library contains complete data.

In either model, neutron collisions at energies less than 5 eV must be simulated using a different data library that takes into account the molecular structure of the material since thermal neutron collisions may transfer energy not just to the target nucleus, but also

to the molecule or lattice in the case of crystals. In this case, a library is required not just for each target isotope but for every molecular structure of each isotope [9].

b. Comparison of Select Physics Lists

The strong dependence on physics lists in GEANT4 led to our first research objective: *Evaluate the physics lists available* in *GEANT4 and determine the suitability for this application*. Although many physics lists are prepackaged with GEANT4 and many more custom physics lists are possible, for our simulation we considered one custom and three reference physics lists. Although there are many differences in models applied for all particles, for the purpose of this work the models and data used in each physics list for neutron and gamma interactions below 20 MeV are of most significance. Figure 3 and Figure 4 show a graphic comparison of the models and cross section data used.

(1) LEND 1.5.1

LEND 1.5.1 is a custom physics list under development at Lawrence Livermore National Laboratory. This physics list uses the LEND model and datasets for both neutron and gamma interactions below 20 MeV.

(2) FTFP_BERT_HP

FTFP_BERT_HP is a reference physics list distributed with GEANT4. This physics list uses the Bertini Cascade model for gamma interactions and the NeutronHP model for neutron interactions below 20 MeV.

(3) Shielding

Shielding is a reference physics list distributed with GEANT4. As in FTFP_BERT_HP, this physics list also uses the Bertini Cascade model for gamma interactions and the NeutronHP model for neutron interactions below 20 MeV.

(4) ShieldingLEND

ShieldingLEND is a reference physics list distributed with GEANT4. This physics list uses a combined LEND and Bertini Cascade model for gamma interactions below 20 MeV. For neutron interactions it uses the LEND model below 20 MeV.

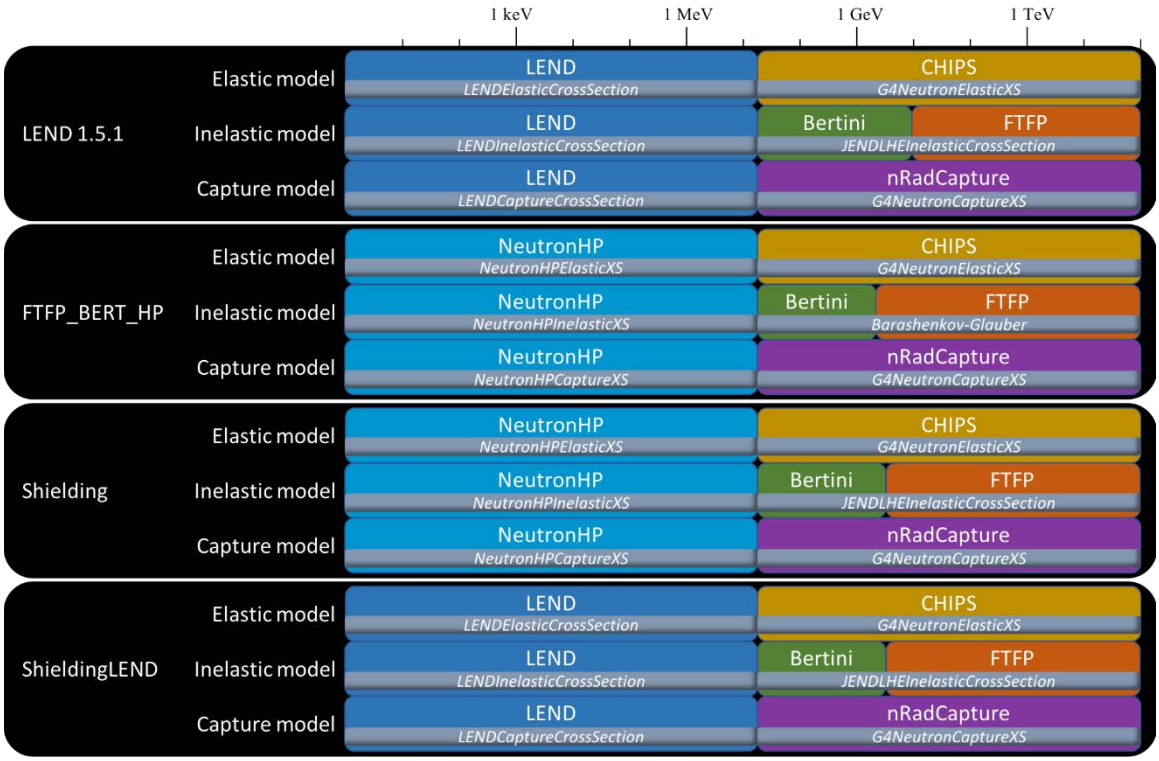

Comparison of neutron processes and cross section datasets used in the GEANT4 physics lists evaluated in this work. Fission processes not shown.

Figure 3. Neutron processes and cross section datasets used in select GEANT4 physics lists. Adapted from [17].

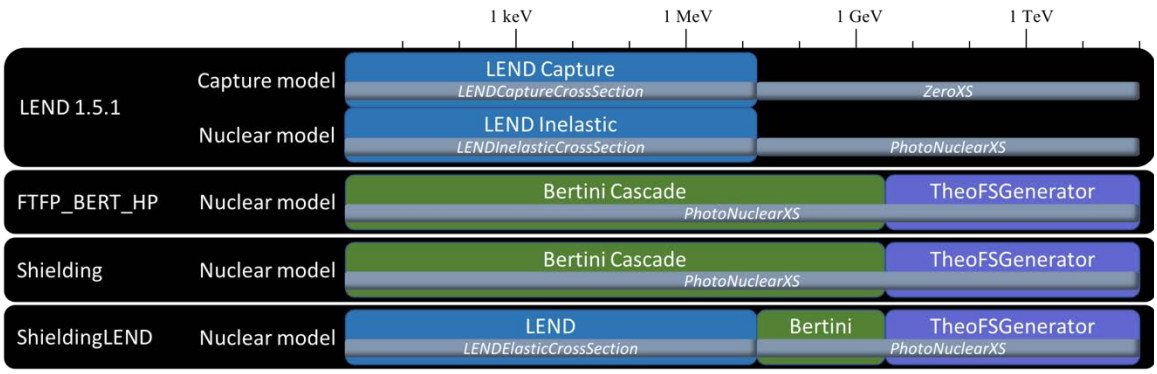

Comparison of gamma processes and cross section datasets used in the GEANT4 physics lists evaluated in this work. Fission processes not shown.

Figure 4. Gamma processes and cross section datasets used in select GEANT4 physics lists. Adapted from [17].

3. Implementation of Optical Photons

None of these physics lists model the production and transport of low energy (optical) photons. GEANT4 treats optical photons and gamma photons as distinct particles with different physics models used for each in the simulation. This enables accurate simulation of the wavelike nature of optical photons. Although there is no absolute distinction between a gamma photon and an optical photon, in general a photon is considered optical if its wavelength is significantly greater than some characteristic length scale (for instance, the lattice spacing) [9].

Implementing optical photons in the simulation can be broken into two parts: registering the physics processes, and defining the necessary material properties. The physics processes are implemented by registering the GEANT4 class *G4OpticalPhysics* in the physics list. This class implements optical photon production through both scintillation and Cerenkov radiation. The material properties are defined in the implementation of the virtual class *G4VPhysicalVolume* [9].

GEANT4 does not simulate the actual lattice structure of a material such as BGO. Optical physics processes are instead simulated based on macroscopic material properties. These properties parameterize scintillation, Cerenkov radiation, bulk absorption,

reflection, refraction, and Rayleigh scattering in the material. Appendix A contains the material properties used in our simulation of BGO.

In theory, if the boundary between two materials is perfectly smooth, the refractive index of each material is sufficient to completely define the behavior of an optical photon at the interface. In practice, the solution due to the imperfect finish of any real surface is much more complex. GEANT4 models the behavior at a boundary by defining a border surface at the interface and assigning optical properties to this surface. The surface finish (e.g., polished, ground, painted) and some surface materials (e.g., Teflon) can be specified using lookup tables (LUT) distributed with GEANT4 [9]. In our simulation, we modelled the BGO crystal as polished and wrapped in Teflon by invoking the *PolishedTeflon_LUT*.

B. SIMULATION GEOMETRY

Our simulation geometry consists simply of a neutron source and a target cylinder coupled to a photon detector, as shown in Figure 5. In general, the target material is modelled as BGO but in some cases it is modelled as pure ^{209}Bi as described in Section IV.A. In all cases, the target is modelled as wrapped in Teflon on all surfaces except the surface adjacent to the photodetector. The dimensions of the target were chosen to recreate the physical BGO sample we have available for testing.

Neutrons incident on the target are modelled as uniformly distributed across the front face normal to the surface. This is representative of a point source at a distance much greater than the diameter of the target. Several neutron energy spectra are modelled, including those from ^{252}Cf and ^{239}Pu-Be sources, as illustrated in Appendix B.

Optical photon transport is modelled within the target, and all optical photons arriving at the photon detector are considered detected. In practice, the photon detector is where the target would be coupled to a PMT, and there would be some inefficiency in the coupling and in the operation of the PMT, which would result in the degradation of the detected signal. Since PMTs are already well characterized, we do not consider these losses in our simulation.

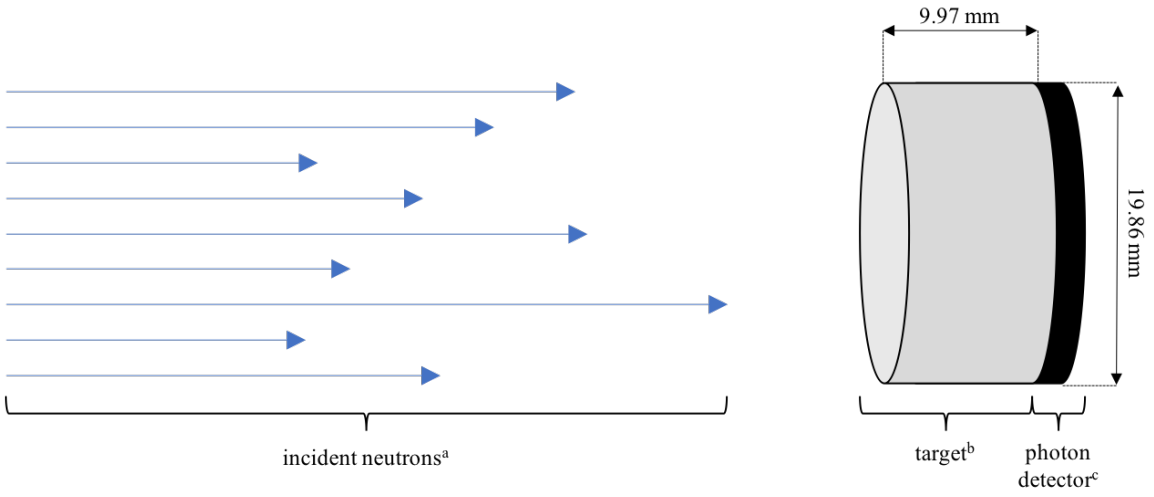

[a] Neutrons incident normal to and distributed uniformly across the front face of the target
[b] Target modelled as monolithic BGO crystal except as noted in Section IV.A. All surfaces of the target except the face adjacent to the detector are modelled as wrapped in Teflon
[c] Optical photons are considered detected when they reach the photon detector

Figure 5. Simulated detector geometry

C. NOT SIMULATED

By design, the simulation does not directly incorporate the crystalline structure of BGO and neglects Mie scattering (an analytical solution to the scattering of photons by particles with dimensions on the order of the photon wavelength). The sources used (^{252}Cf and ^{239}Pu-Be) are simulated as pure neutron sources with no gamma component.

1. Crystalline Structure of BGO

Although the *G4Material* class used to define the material in a GEANT4 simulation contains information of the relative abundance of its constituent elements and macroscopic information such as temperature, pressure, density, and physical state [9], it does not contain information about the internal crystalline structure. In our simulation we use the *G4_BGO* material class provided with the GEANT4 distribution and simulated under standard conditions. Behavior that relies on the crystalline structure, such as optical photon transport, is instead modelled by defining the macroscopic properties listed in Appendix A.

2. Mie Scattering

In general, Mie scattering is an analytical solution for scattering of photons by geometries with a spherical target where the sphere radius is on the order of the photon wavelength [9]. The optical wavelengths of interest in our simulation are the scintillation distribution of BGO, which is between 350 and 750 nm (Appendix A). In our simulation, there are no particles of this size and so we can safely ignore Mie scattering as negligible.

3. Gamma Emission of Neutron Sources

Only the neutron emission is simulated for sources reproduced in the simulation (^{252}Cf and ^{239}Pu-Be). The gamma component is explicitly not simulated in order to focus the results on optical photon production due to neutron radiation incident on the detector. This represents a detector that is perfectly shielded from gamma radiation.

D. DATA COLLECTION

Data is collected in GEANT4 during the simulation. Although some elementary analysis is conducted in GEANT4 during the simulation, most of the data is stored using the ROOT framework for later analysis. GEANT4 also poses some challenges to collecting the data needed for our analysis.

1. Data Collection Design

Data collection occurs in the implementation of *G4VSensitiveDetector* in our simulation. Although GEANT4 contains several tools for data collection and analysis, we chose to use the ROOT toolkit developed at CERN to collect and analyze the data generated in GEANT4. ROOT is uniquely developed by physicists for physicists to store and analyze large amounts of data.

Data is collected in GEANT4 in an object-oriented framework. A *G4VHit* object is implemented in *DetectorHit* to store data for each particle interaction (referred to as a hit) in the BGO material (referred to as the detector). *DetectorHits* associated with a given particle (referred to as a track) are stored in a *DetectorTrack* object containing information unique to that track. Photons produced are stored in *PhotonTrack* objects. *DetectorTracks*

and *PhotonTracks* associated with the current simulation event are stored in a *HitCollection* object. At the end of each event, the *HitCollection* is parsed into ROOT *TTree* data structures and histograms. At the end of the simulation, these are saved in two ROOT *TFiles* for further analysis.

2. Data Collection Challenges

Although GEANT4 is a powerful software package, it does pose some challenges to collecting the data we need. In particular, secondaries produced in an interaction are not easily correlated to later tracks, and the reaction subtype as defined by GEANT4 does not clearly differentiate between inelastic collisions and other interactions such as *(n,2n)* reactions.

a. Associating Reaction Secondaries with Their Tracks

In a given reaction, GEANT4 determines which (if any) secondary particles are produced and stores these products as a vector of *G4Tracks*. These tracks are incorporated into the simulation and continue on their own trajectory to become part of the GEANT4 simulation. However, the secondary tracks are not assigned a track number when they are created as secondaries, but rather are only assigned a track number at a later step when GEANT4 begins to simulate the life of that particle. Each track does contain the track number of its parent track, but since the parent track may have many reactions in its life, there is no concise method to determine precisely which reaction resulted in the current track.

This correlation is significant in our simulation since the incident neutrons do not themselves generate photons and we are interested in the chain of reactions from incident neutron to photon production and ultimately photon detection. In order to correlate each track with the reaction that generated that particular particle, we implement a concrete class inheriting from *G4VUserTrackInformation*. Using this class, we can store a pointer to the progenitor hit that resulted in the given secondary.

b. Determining Reaction Subtype

GEANT4 bins reaction by type (e.g., hadronic, electromagnetic, optical). Hadronic processes are further binned by subtype, and each subtype is assigned an integer identifier (elastic=111, inelastic=121, capture=131, etc.). However, the inelastic subtype would more appropriately be named "other" as it includes all reactions that are not elastic, capture or fission. In order to get greater fidelity on the reaction subtype, we analyze the secondaries produced in each so-called inelastic reaction and use this data to assign our own reaction subtype. In this new numbering scheme, each digit represents the number of a particular particle type produced in the reaction as illustrated in Figure 6. In this way, we can differentiate between all the possible reaction subtypes.

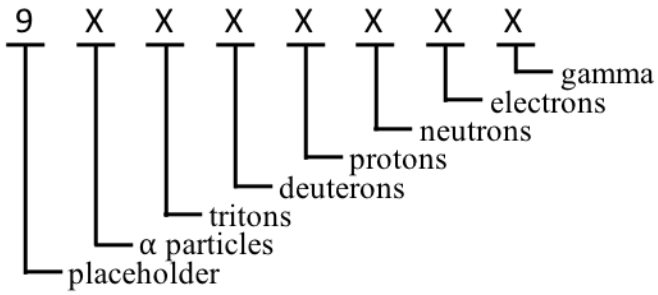

Figure 6. Reaction subtype numbering schema.

Determining the reaction subtype is further complicated by the way GEANT4 determines each simulation step length. At the start of each step in the simulation, each active process proposes a step length. GEANT4 implements the shortest step length. The user must be aware that the process that defined the step in this way is not the only process that can occur during the step as all active processes will still be invoked. The actual process that produced a secondary should be accessed by the track *GetCreatorProcess* method.

E. CONCLUSION

We have constructed a simulation in GEANT4 using four different physics lists (LEND1.5.1, FTFP_BERT_HP, Shielding, and ShieldingLEND) in order to model the

optical response of BGO to incident neutron radiation. In the following chapter, we validate the simulation using sets of known data and use the simulation results to select a physics list, quantify neutron interactions in BGO, and evaluate subsequent photon production.

THIS PAGE INTENTIONALLY LEFT BLANK

IV. SIMULATION RESULTS

We conducted two sets of simulations. In the first set we conducted three simulation runs. The objective of these runs was to validate the simulation design by comparing the results to sets of independent known data. During these runs we also evaluated the results based on each of the four physics lists in order to determine the most appropriate physics list to implement for our simulation (research objective 1). In the second set we conducted several runs to collect the data necessary to quantify the neutron interactions in BGO (research objective 2) and evaluate the reaction channels from incident neutron to optical photon production (research objective 3).

A. VALIDATION RESULTS

We compared simulation results to three sets of known data to validate the simulation design and compare the behavior of the four physics lists. First, we ran a simulation to duplicate the ENDF cross sections for a pure ^{209}Bi target. Second, we ran a simulation to duplicate resonant capture measurements conducted by Domingo-Pardo et al. at CERN [18]. Finally, we ran a simulation to duplicate our own experimental results (presented in Section IV.A.3). Based on these simulations we concluded that the simulation design is valid and that all four physics lists considered perform well in this application. However, LEND 1.5.1 and ShieldingLEND more closely matched experimental results in the cross section validation and the experimental comparison.

1. ENDF Cross Section

Using each physics list, we simulated 10^9 neutrons incident on a ^{209}Bi target from a 14.1MeV isotropic source. We calculated the resulting cross section and compared it to the accepted values from ENDF/B-VIII [3] using

$$\sigma = \frac{-1}{\rho D} \ln\left(\frac{N - N_s}{N}\right), \tag{5}$$

where N is the number of incident neutrons, N_s is the number of scattered neutrons, ρ is the atomic density of ^{209}Bi atoms, and D is the target depth [19]. Assuming a standard counting uncertainty, the standard error in the cross section was calculated by the propagation of the uncertainty in N_s using

$$\delta\sigma = \frac{\partial\sigma}{\partial N_s}\delta N_s = \frac{\sqrt{N_s}}{\rho D\left(N - N_s\right)}. \tag{6}$$

derived from [20]. Although the simulation results are close to the expected value for all physics lists as shown in Table 1, we found that the cross section is outside one standard error for total reactions, elastic scattering, inelastic scattering, and *(n,2n)* when using the FPTP_BERT_HP and Shielding physics lists. It is worth noting that the standard error in these cases is exceptionally small due to the high number of incident neutrons. As such, although outside of one standard error, these results are still within a fraction of a percent of the accepted values. The preferred physics lists based on the cross section validation are LEND 1.5.1 and ShieldingLEND.

2. Resonant Capture

Our second validation analysis was to compare the simulation behavior with experimentally observed resonant energies by simulating an isotropic neutron source with a linear energy distribution from 0.01 to 5 keV and a ^{209}Bi target. Resonant neutron capture occurs when the incident neutron energy corresponds to an excited state of the target nucleus. Simulation in GEANT4 reproduced resonance peaks (shown in red in Figures 7 through 10) that closely match the resonant energies experimentally observed in ^{209}Bi by the CERN neutron Time of Flight (nTOF) collaboration [18]. As expected, the four physics lists considered performed similarly with all simulated peaks within 1.10% of the experimental value.

Table 1. Comparison of ENDF/B-VIII cross sections and simulation cross sections from the four physics lists

process	ENDF/B-VIII [3]	LEND 1.5.1	FTFP_BERT_HP	Shielding	ShieldLEND
total	5.35908	5.3591 ±0.00048981 (0.0733 σ)	5.3498 ±0.00048929 (-19.0 σ)	5.3495 ±0.00048927 (-19.6 σ)	5.3587 ±0.00048978 (-0.836 σ)
elastic	2.82265	2.8221 ±0.0046369 (-0.126 σ)	2.8027 ±0.0046024 (-4.34 σ)	2.8026 ±0.0046027 (-4.35 σ)	2.8225 ±0.0046389 (-0.0256 σ)
inelastic	0.38615	0.38626 ±0.00087519 (0.118 σ)	0.38794 ±0.00087898 (2.03 σ)	0.3879 ±0.00087898 (1.99 σ)	0.38634 ±0.00087537 (0.211 σ)
n,γ	1.0200×10^{-3}	0.0010061 $\pm4.1454\times10^{-5}$ (-0.336 σ)	0.0010146 $\pm4.17\times10^{-5}$ (-0.129 σ)	0.0010231 $\pm4.1876\times10^{-5}$ (0.0734 σ)	0.0010245 $\pm4.1836\times10^{-5}$ (0.107 σ)
n,2n	2.1445	2.145 ±0.003191 (0.167 σ)	2.1534 ±0.0032147 (2.76 σ)	2.1532 ±0.0032147 (2.71 σ)	2.144 ±0.0031897 (-0.152 σ)
n,p	9.2800×10^{-4}	0.00092261 $\pm3.9697\times10^{-5}$ (-0.144 σ)	0.00094122 $\pm4.0163\times10^{-5}$ (0.321 σ)	0.00092695 $\pm3.986\times10^{-5}$ (-0.0347 σ)	0.00093514 $\pm3.9969\times10^{-5}$ (0.17 σ)
n,p n	2.7234×10^{-3}	0.0027302 $\pm6.8313\times10^{-5}$ (0.100 σ)	0.0027389 $\pm6.8536\times10^{-5}$ (0.227 σ)	0.0027319 $\pm6.8452\times10^{-5}$ (0.125 σ)	0.002731 $\pm6.8327\times10^{-5}$ (0.111 σ)
n,d	2.2700×10^{-4}	0.00022755 $\pm1.9712\times10^{-5}$ (0.00514 σ)	0.00022744 $\pm1.9741\times10^{-5}$ (-0.00023 σ)	0.00022467 $\pm1.9621\times10^{-5}$ (-0.141 σ)	0.00022551 $\pm1.9625\times10^{-5}$ (-0.0988 σ)
n,d n	8.8000×10^{-8}	7.6913×10^{-8} $\pm3.6239\times10^{-7}$ (-0.0306 σ)	1.5381×10^{-7} $\pm5.1333\times10^{-7}$ (-0.0663 σ)	3.8451×10^{-8} $\pm2.5668\times10^{-7}$ (-0.193 σ)	3.8456×10^{-8} $\pm2.5627\times10^{-7}$ (-0.193 σ)
n,t	6.9200×10^{-5}	7.026×10^{-5} $\pm1.0953\times10^{-5}$ (0.0968 σ)	6.8482×10^{-5} $\pm1.0832\times10^{-5}$ (-0.0663 σ)	7.1058×10^{-5} $\pm1.1034\times10^{-5}$ (0.168 σ)	6.9144×10^{-5} $\pm1.0867\times10^{-5}$ (-0.00514 σ)
n,t n	8.3728×10^{-8}	7.6913×10^{-8} $\pm3.6239\times10^{-7}$ (-0.0188 σ)	1.1535×10^{-7} $\pm4.4455\times10^{-7}$ (0.0711 σ)	7.6903×10^{-8} $\pm3.63\times10^{-7}$ (-0.0188 σ)	–
n,α	7.3700×10^{-4}	0.00073302 $\pm3.5383\times10^{-5}$ (-0.107 σ)	0.00074673 $\pm3.5772\times10^{-5}$ (0.278 σ)	0.00073077 $\pm3.539\times10^{-5}$ (-0.17 σ)	0.00073532 $\pm3.5441\times10^{-5}$ (-0.0415 σ)
n,α n	7.4917×10^{-5}	7.4759×10^{-5} $\pm1.1298\times10^{-5}$ (-0.0139 σ)	7.2443×10^{-5} $\pm1.1141\times10^{-5}$ (-0.222 σ)	7.6403×10^{-5} $\pm1.1442\times10^{-5}$ (0.13 σ)	7.1567×10^{-5} $\pm1.1055\times10^{-5}$ (-0.303 σ)

Comparison of ENDF/B-VIII and simulation cross section of reactions for 14.1 MeV neutrons incident on ^{209}Bi. Number in parenthesis indicates the deviation in multiples of standard error of the simulation results from the ENDF/B-VIII accepted value. Results highlighted in red are not within one standard error of the accepted value. All cross section values are in barns.

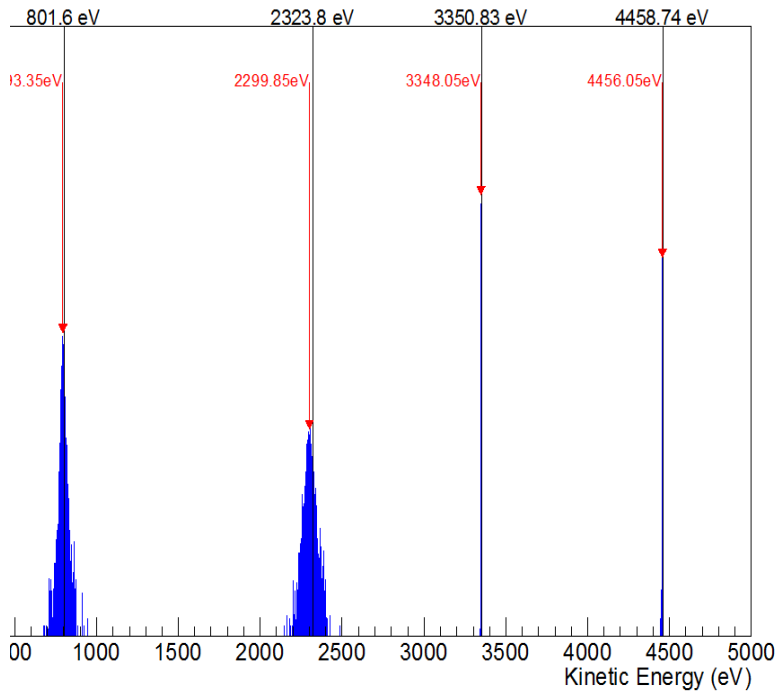

Figure 7. Simulation of a linear spectrum of 10^8 neutrons from 0.01 eV to 5 keV incident on ^{209}Bi using the LEND 1.5.1 physics list

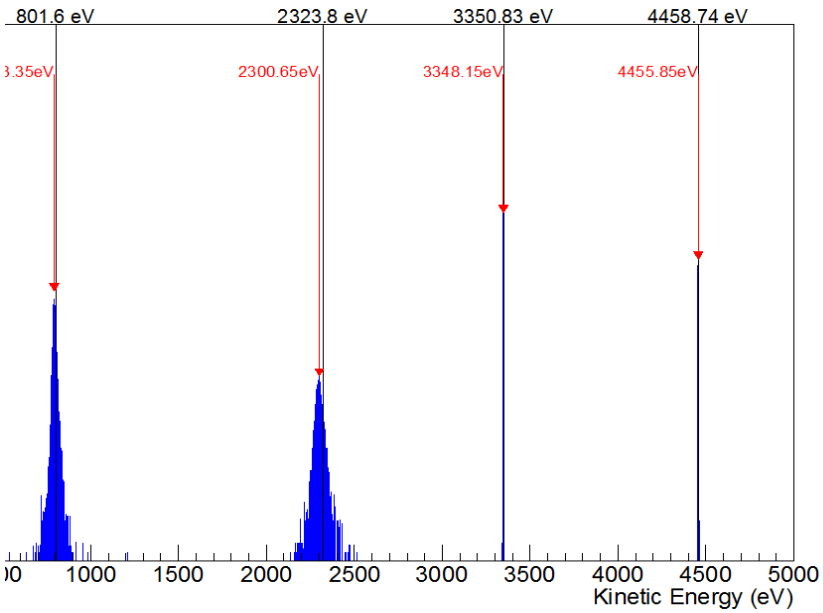

Figure 8. Simulation of a linear spectrum of 10^8 neutrons from 0.01 eV to 5 keV incident on ^{209}Bi using the FTFP_BERT_HP physics list

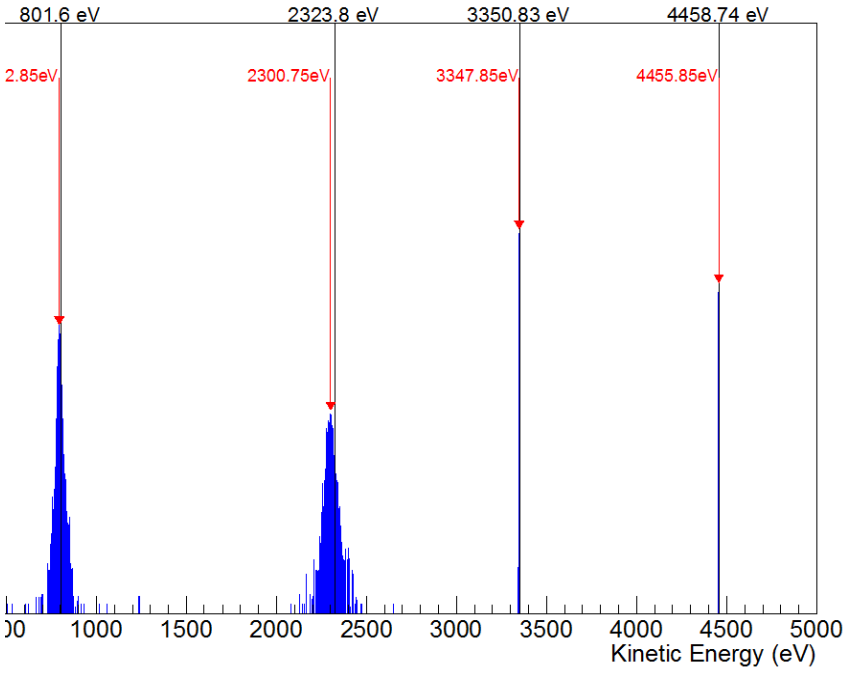

Figure 9. Simulation of a linear spectrum of 10^8 neutrons from 0.01 eV to 5 keV incident on ^{209}Bi using the Shielding physics list

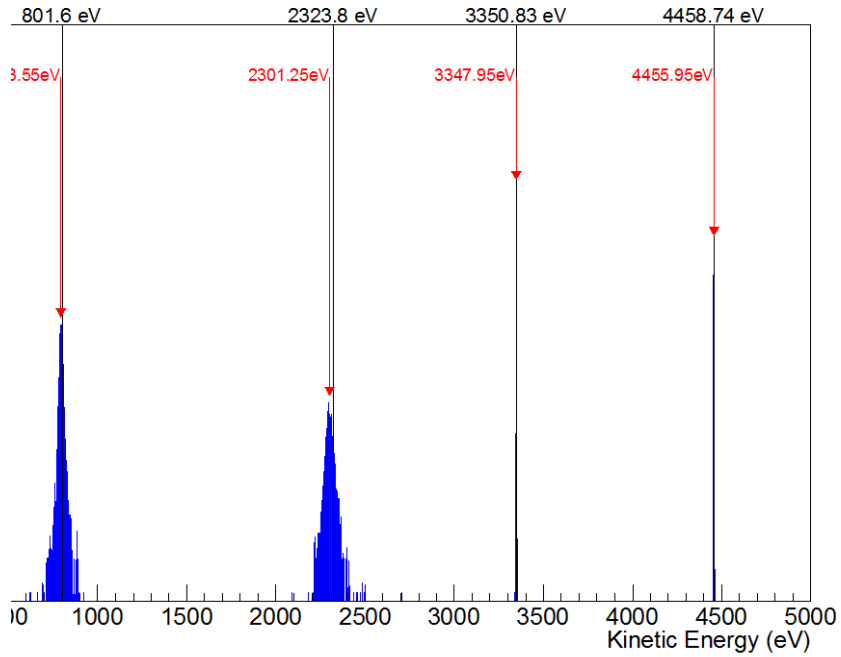

Figure 10. Simulation of a linear spectrum of 10^8 neutrons from 0.01 eV to 5 keV incident on ^{209}Bi using the ShieldingLEND physics list

3. Experimental Results of BGO and BGO-based ZEBRA Detectors Exposed to ^{252}Cf and ^{239}Pu-Be Sources

In order to compare simulation output with real world results, we attempted to recreate the experiments by Ryzhikov et al. [2] in the lab and, in the case of the single BGO crystal, in the simulation. Two detectors were assembled. The first consisted of a single crystal of BGO (19.86mm diameter x 9.97mm thick) wrapped in Teflon and coupled to a PMT. The second consisted of a multilayer BGO-based ZEBRA scintillator (39.97mm x 40.07mm x 40.71mm deep) coupled to an identical PMT. 50mm of lead shielding was used to attenuate gamma radiation on the detectors as shown in the experimental setup in Figure 11. The experimental setup was calibrated using a ^{137}Cs source.

Two neutron sources were used. The ^{239}Pu-Be source used had an output neutron flux of 1.70×10^{6} nps and was positioned 250 mm from the front face of each detector. The ^{252}Cf source used had an output neutron flux of 3.91×10^{4} nps and was positioned 125 mm from the front face of each detector. A background spectrum was collected and subtracted from the measured results for comparison to the simulated data.

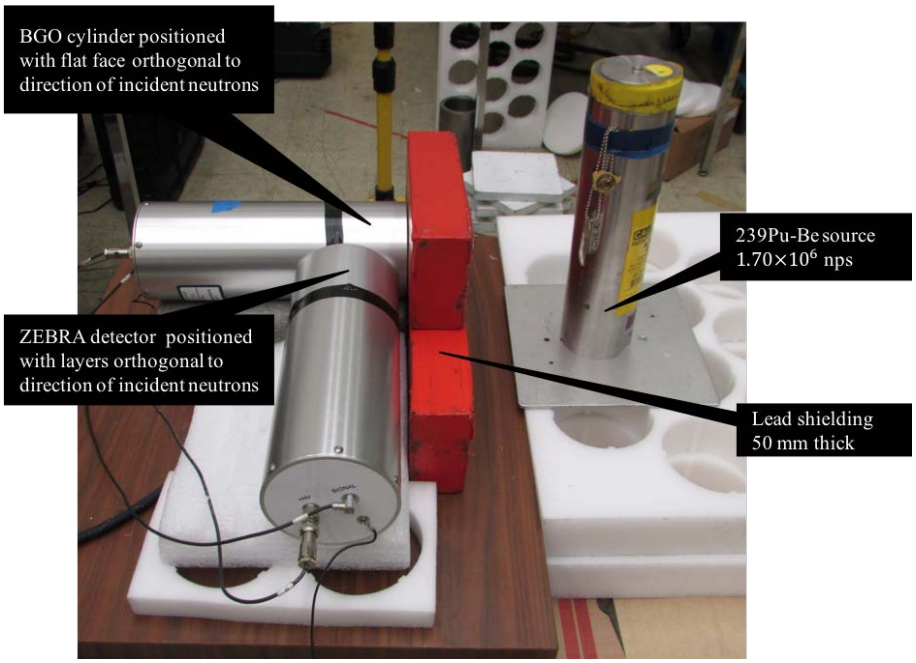

Figure 11. Experimental setup for exposure of BGO and BGO-based ZEBRA detectors to ^{239}Pu-Be source.

The data acquisition schema is shown in Figure 12. Each detector was wrapped in Teflon and coupled to separate PMTs using optical gel. Each PMT was connected to an individual preamplifier and amplifier. Both amplifiers were connected to a single multichannel buffer.

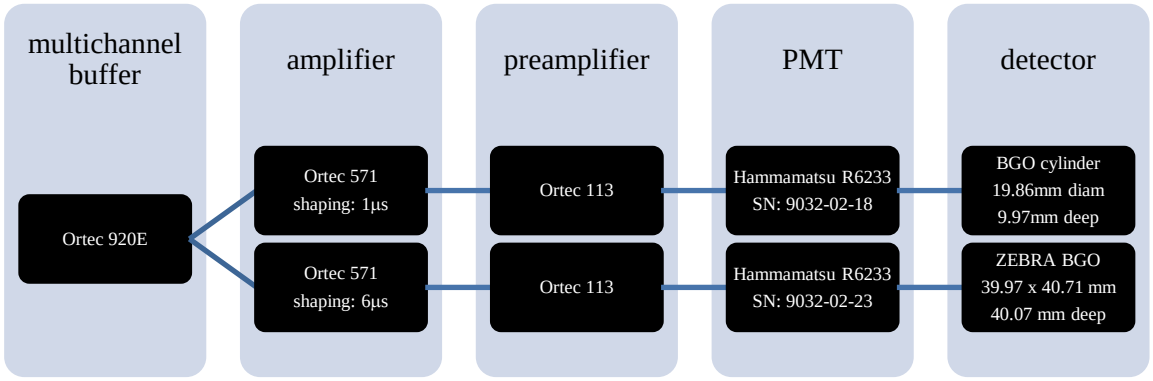

Figure 12. Data acquisition for experimental setup.

The simulation for the BGO cylinder was designed to produce the same total neutron flux on the detector as in the experimental measurements. Neutron spectra used for the sources in the simulation are illustrated in Appendix B. The results of both the experiment and the simulation for BGO exposed to ^{252}Cf and ^{239}Pu-Be sources were normalized to the integral under the curve and plotted in Figure 14 and Figure 15.

In order to simulate the pulse shaping of the experimental setup, the simulated time of arrival of each photon at the photodetector is recorded in an array. The timeline is divided into windows each the length of the selected pulse shaping time to emulate the pulse shaping of the Ortec 571. The number of photons arriving in a given window corresponds to the amplitude of a single pulse. Each pulse is then binned in a histogram according to pulse amplitude. As in the experimental setup, the simulated pulse shaped output is correlated to an energy by simulating a ^{137}Cs source and using a linear fit to scale the pulse amplitude such that the peak in the simulated pulse-shaped output is aligned with the 662 keV peak characteristic of ^{137}Cs. As is apparent in Figure 13, all four physics lists performed similarly in the calibration and although the 662 keV peak is well aligned with

the expect value, the behavior at energies between 200 and 600 keV does not closely follow the experimental data.

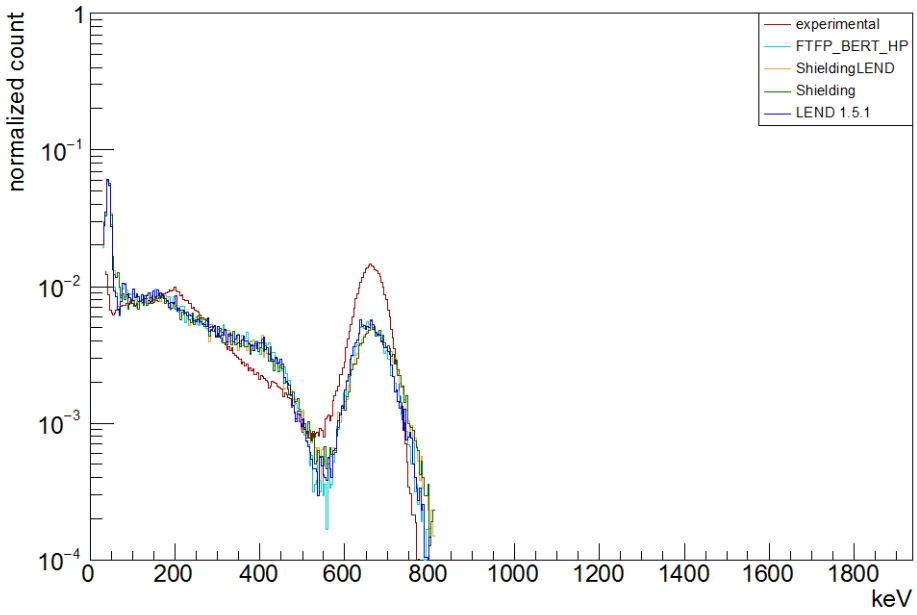

Figure 13. Calibration of simulation output using a ^{137}Cs source.

Using the calibration parameter determined with the ^{137}Cs simulation, ^{252}Cf and ^{239}Pu-Be neutron sources were simulated using each of the four physics lists. In the case of ^{252}Cf (Figure 14), the experimental data shows no characteristic peaks. However, the total count was low and such peaks may be obscured in the background noise. In contrast, FTFP_BERT_HP and Shielding physics lists produced pronounced peaks at 550 keV and 870 keV. ShieldingLEND and LEND 1.5.1 physics lists more closely match the experimental data. In the case of ^{239}Pu-Be (Figure 15), the experimental data does show two peaks at 495 keV and 820 keV. The FTFP_BERT_HP and Shielding physics lists produce peaks at 564 keV and 862 keV while the ShieldingLEND and LEND 1.5.1 physics lists produce a single broad peak at 635 keV.

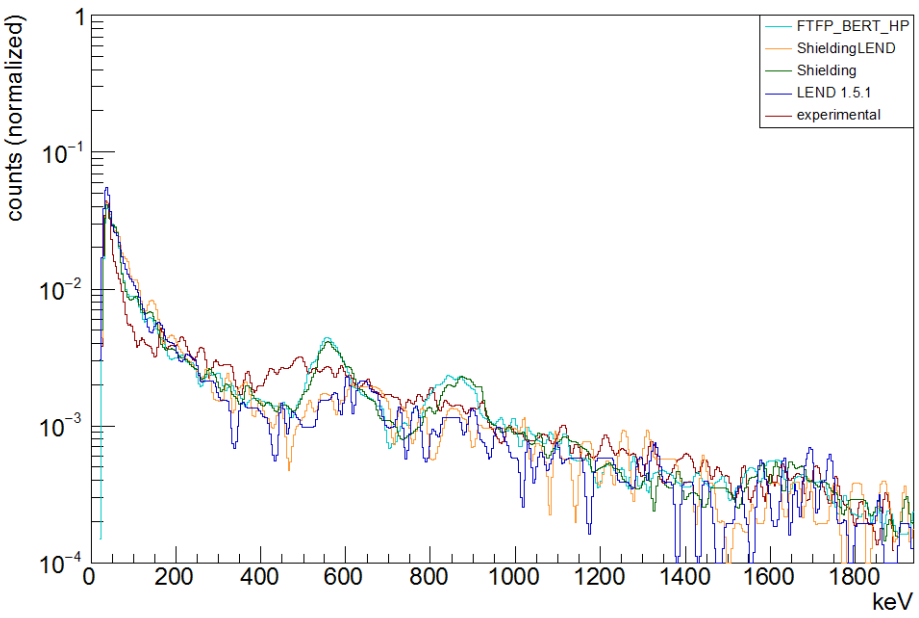

Figure 14. Comparison of lab and simulation results for BGO response to ^{252}Cf neutron source

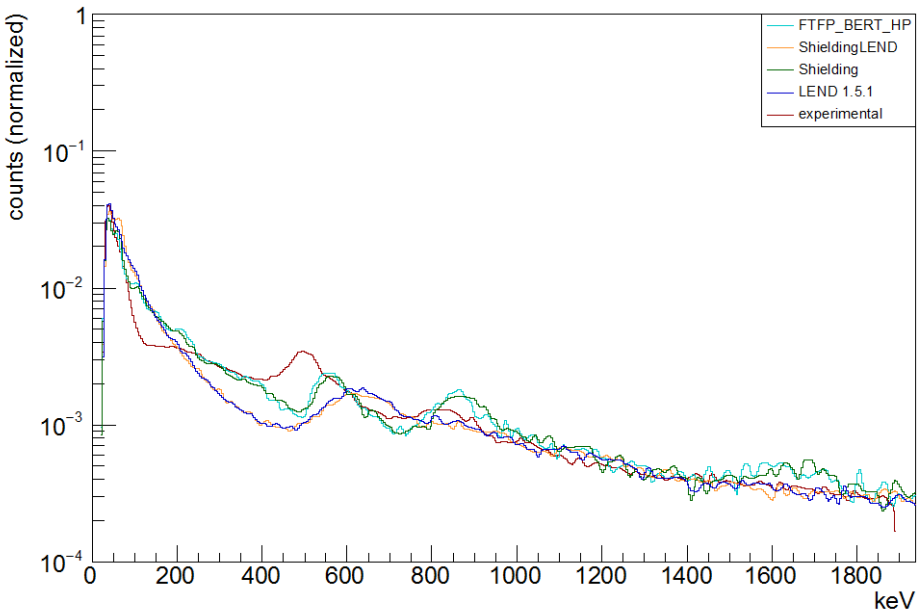

Figure 15. Comparison of lab and simulation results for BGO response to ^{239}Pu-Be neutron source

Both the simulation and the experimental method require further refinement in order to draw a complete conclusion regarding the validity of the simulation. The ^{252}Cf experiment did not accumulate sufficient counts to identify any characteristic peaks to compare with the simulation data. This experiment should be repeated with longer run time to more clearly compare with the simulation data and better understand the behavior of the BGO under neutron exposure. Based on the spectra of ^{252}Cf and ^{239}Pu-Be, we expected to see some common peaks in the two experiments. For example, both experiments should have a 511 keV peak associated with pair production.

In the experimental setup, the PMT was shielded only on the side facing the neutron source and so gamma photons may be introduced into the detector through scattering or through neutron interactions with other materials in the laboratory. For example, neutron inelastic scattering with iron produces a 850 keV gamma photon and we see a peak in the experimental data near the same value [21]. Either a simulation with combined gamma and neutron flux or an experiment with additional shielding may yield a closer match between experiment and simulation.

The simulation does not account for the efficiency of the PMT or the response functions of both the PMT and the preamplifier. These response functions would tend to disperse the detected signal in time and as such affect the pulse shape. These two response functions should be incorporated into the simulation by convolution with the array of photon detection times prior to performing the pulse shaping operation.

Comparison between the BGO crystal and BGO-ZEBRA detector signals in Figure 16 and Figure 17 reveals that the BGO crystal had a significantly stronger response at all but the lowest energies despite the ZEBRA detector having a significantly larger cross sectional area. Since the percentage of BGO in the ZEBRA detector is unknown, the response could not be normalized to the volume of heavy oxide scintillator in each detector and thus the results are not directly comparable, but it is worth noting that in this particular experiment, the cross section area of the BGO crystal (309.8mm^2) is less than 20% of that of the BGO-ZEBRA (1602 mm^2).

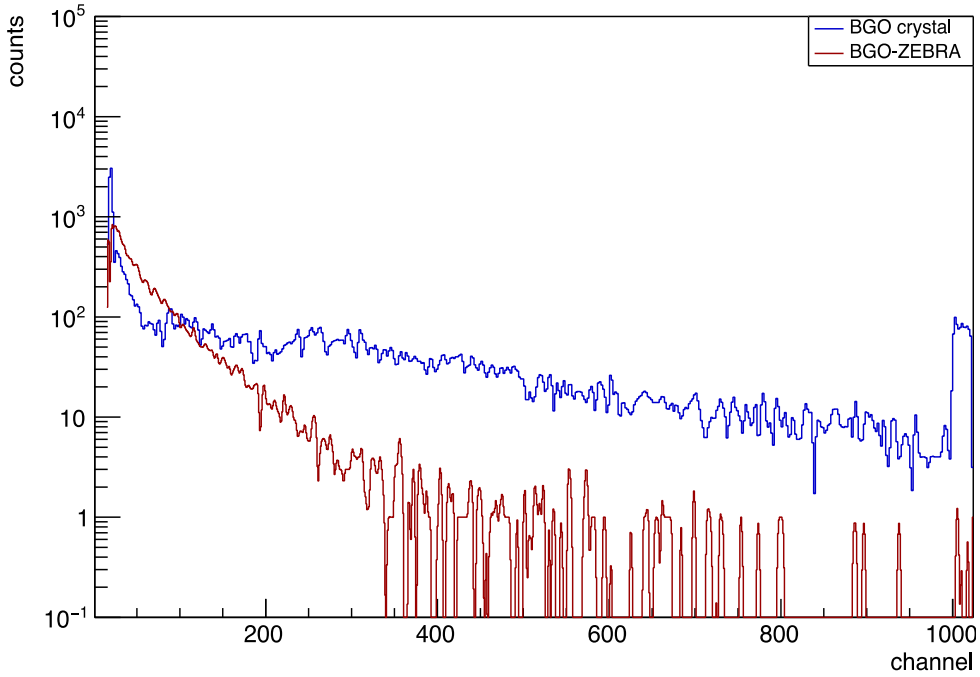

Figure 16. Comparison of experimental results for BGO and BGO-ZEBRA response to ^{252}Cf neutron source

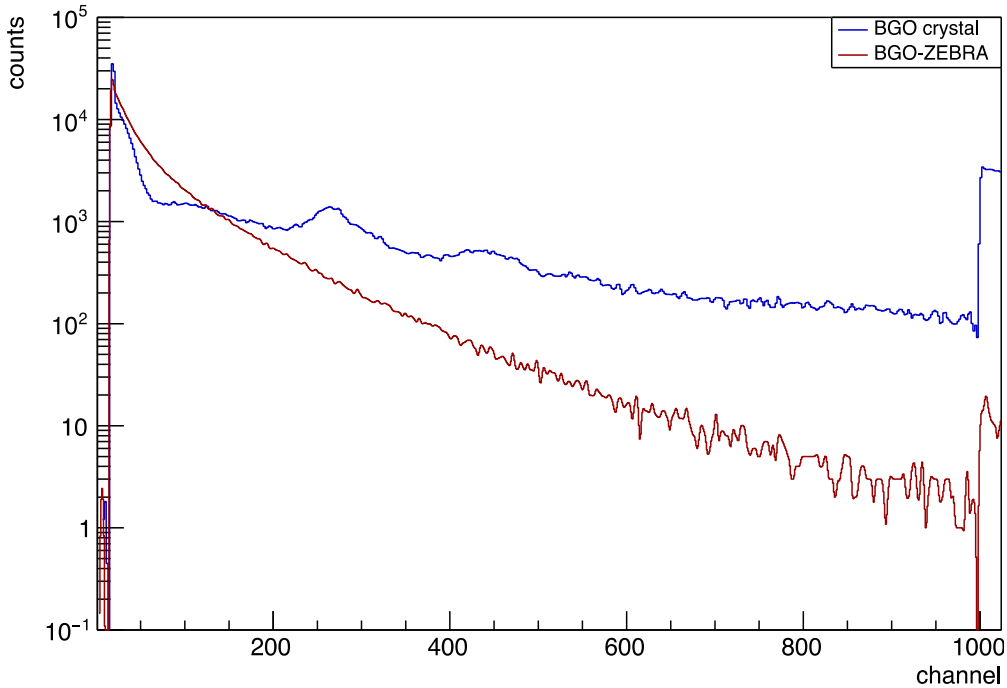

Figure 17. Comparison of experimental results for BGO and BGO-ZEBRA response to ^{239}Pu-Be neutron source

B. RESEARCH RESULTS

With the validation complete, we conducted two research simulations collecting data to quantify the neutron interactions in BGO (research objective 2) and evaluate the reactions leading from incident neutron to optical photon production (research objective 3). These runs were conducted using the LEND 1.5.1 physics list. The first run simulated 10^7 incident neutrons with a ^{252}Cf neutron source spectrum (equivalent to a 45-hour exposure to a 3.91×10^4 nps source at 125mm) and the second run simulated 10^7 incident neutrons with a ^{239}Pu-Be source (equivalent to a 1 hour exposure to a 1.70×10^6 nps source at 125mm). Neutron spectra used for the sources in the simulation are illustrated in Appendix B.

1. Contribution by Neutron Reaction Channel

As was suggested by Ryzhikov et al. [1], we observed that elastic and inelastic neutron scattering is responsible for the majority of photon production with other interactions such as neutron capture, *(n,α)*, and *(n,2n)* producing significantly fewer photons overall. However, photon production varies significantly based on the incident neutron spectra. Unsurprisingly, we see greater photon production due to elastic scattering and neutron capture in the simulation of ^{252}Cf exposure (Figure 18) than in the ^{239}Pu-Be exposure (Figure 19), likely due to the lower energy spectrum of ^{252}Cf. Conversely, we observe increased photon production due to inelastic scattering and, to a lesser extent, other channels, such as *(n,2n)*, *(n,α)* and *(n,p)* in the ^{239}Pu-Be exposure, which can be explained by the higher energy neutrons produced by the ^{239}Pu-Be source.

Normalizing the number of photons resulting from each neutron process to the number of occurrences of the process (Table 2), we observe that neutron capture and *(n,p)* each produce an order of magnitude more optical photons per neutron interaction than any other process. Despite this, these two processes contribute relatively little to the overall detection signal because of the low cross section of the neutron reaction. For instance, at 1MeV in ^{209}Bi the cross section for neutron capture is 2.7800×10^{-3} barns and for *(n,p)* is 7.7003×10^{-7} barns, while the cross section for elastic scattering is 5.1347 barns [3].

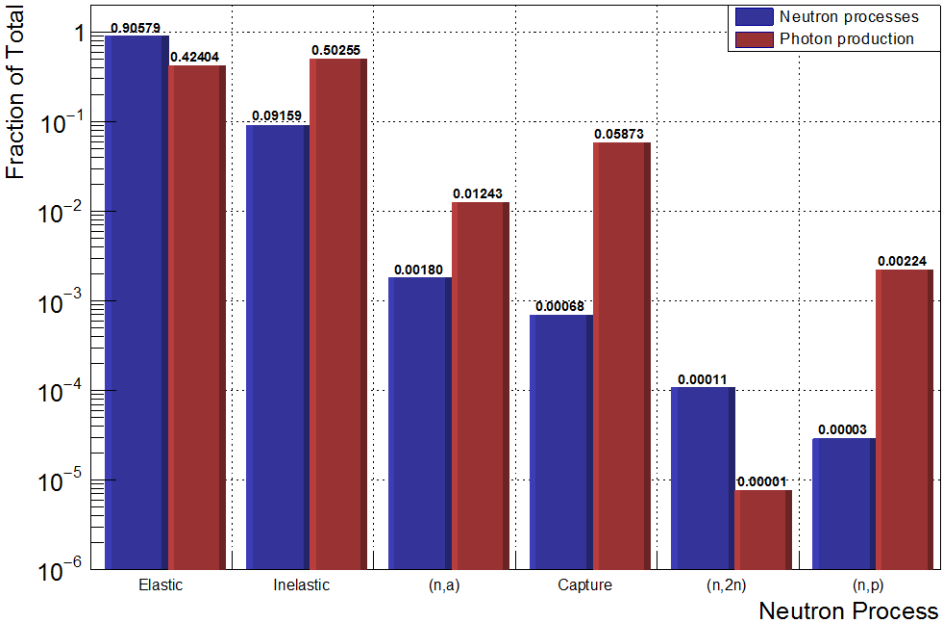

Figure 18. Neutron processes and associated photon production in BGO simulated exposure to ^{252}Cf source

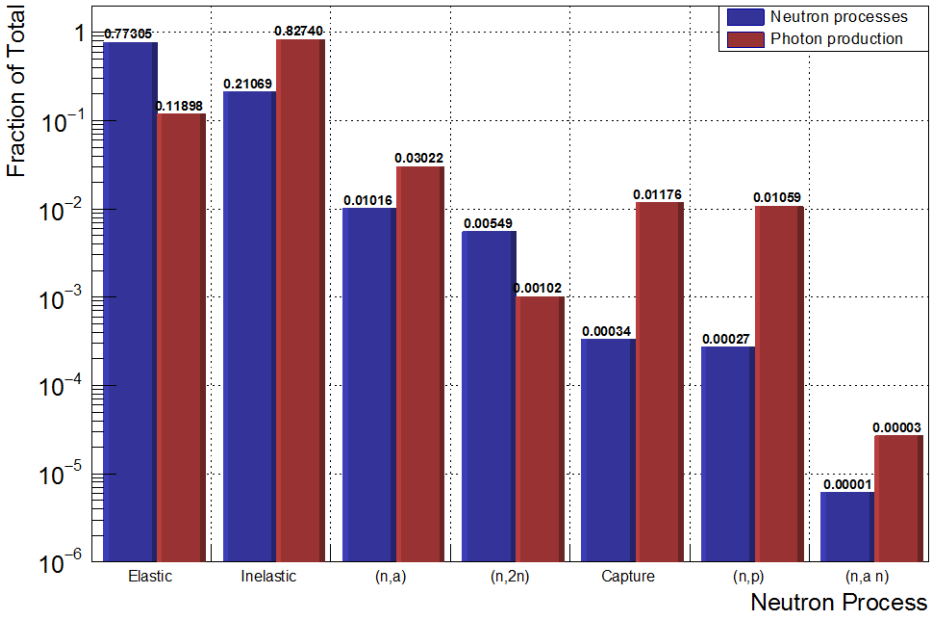

Figure 19. Neutron processes and associated photon production in BGO simulated exposure to ^{239}Pu-Be source

Table 2. Average number of optical photons produced per neutron reaction

process	^{252}Cf	^{239}Pu-Be
elastic	30	30
inelastic	350	762
capture	5490	6791
n,2n	5	36
n,p	4950	7479
n,α	441	577
n,α n	0	835

2. Optical Photon Production Channels

Since neutrons are neutral particles, they do not directly produce optical photons but rather a neutron interaction may result in a chain of succeeding reactions. Some of these reactions will produce optical photons. For simplicity, we will refer to the chain of reactions from incident neutron to optical photon production as the optical photon production channel. In general, these production channels are complex and varied, but using a python script we analyzed the simulation data to identify which channels were most prevalent. The production channel of each photon produced was quantified using an ordered list of the reaction subtypes (as described in Section III C) for each reaction from the incident neutron to the photon production. Each unique list was used to create a key, the incidence of each key was counted, and the results sorted. In this way we could identify those channels with the greatest impact on photon production.

In BGO exposed to a ^{252}Cf neutron spectrum, 99.6% of total photon production was by scintillation and the remainder by Cerenkov radiation. We identified 200 unique optical photon production channels; however, just 13 of these channels are responsible for a cumulative 90% of optical photon production (Figure 20). Two of these channels account for more than half of all optical photon production. The most prominent channel is neutron elastic scattering followed by scintillation (Figure 21). This channel produced 32% of all optical photons. The second leading production channel accounts for 19% of the optical

photons through neutron inelastic scattering resulting in a gamma photon that undergoes Compton scattering yielding an electron that results in Cerenkov radiation of optical photons (Figure 22).

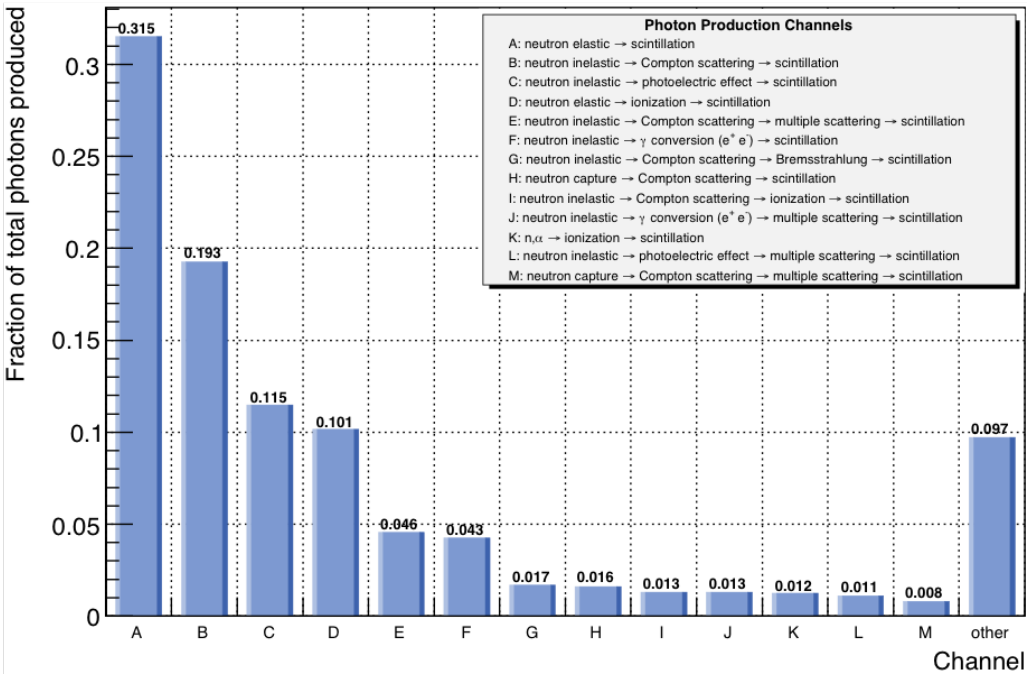

Figure 20. Photon production channels in simulated exposure of BGO to a ^{252}Cf neutron spectrum

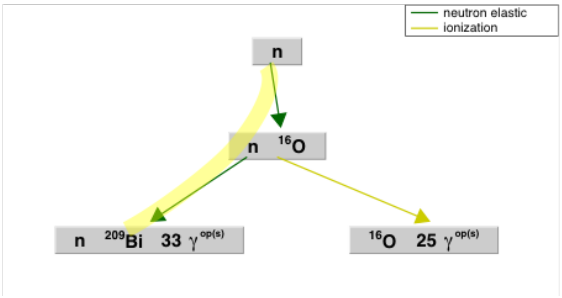

Photon production channel A (highlighted in yellow) is neutron elastic scattering followed by scintillation of optical photons (labelled $\gamma^{op(s)}$). Note that channel D is also present in this event. Each color-coded arrow represents a single reaction. Each arrow starts on the particle undergoing the reaction and ends on a gray block containing the resulting secondaries. As such, the first reaction in this event is elastic scattering of a neutron by ^{16}O (not shown) resulting in a neutron and ^{16}O. The neutron then undergoes elastic scattering by ^{209}Bi resulting in a neutron, ^{209}Bi, and 33 optical photons from scintillation.

Figure 21. An event exhibiting photon production channel A in BGO exposed to a ^{252}Cf source

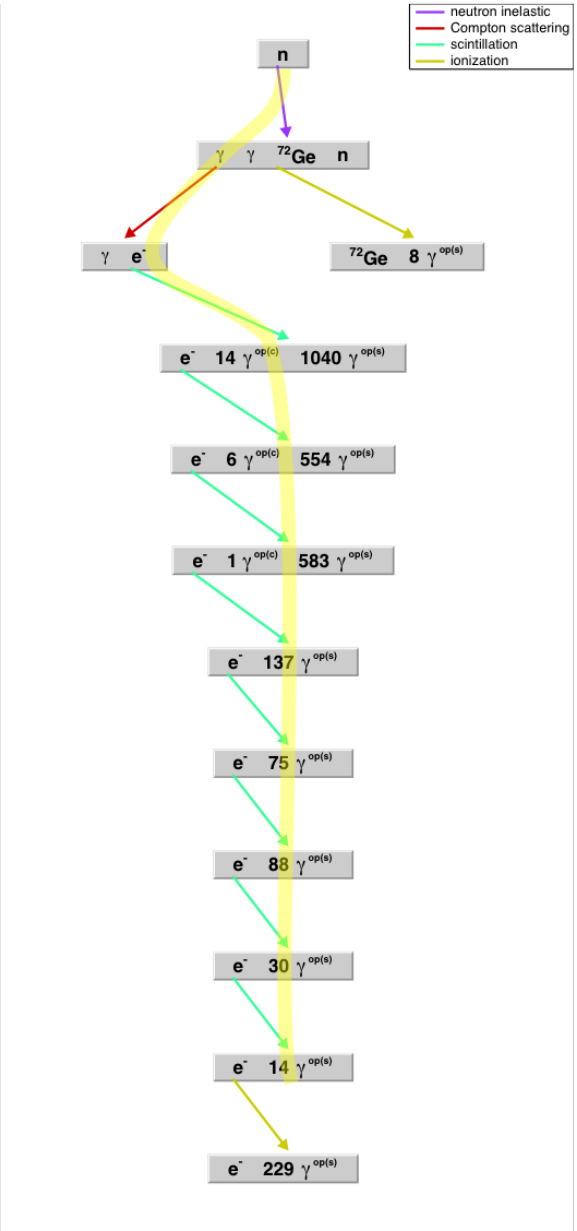

Photon production channel B (highlighted in yellow) is neutron inelastic scattering resulting in a gamma photon that undergoes Compton scattering. The resulting electron produces optical photons through scintillation (labelled $\gamma^{op(s)}$) and, to a lesser extent, Cerenkov radiation (labelled $\gamma^{op(c)}$). Note that channel D is also present in this event. Each color-coded arrow represents a single reaction. Each arrow starts on the particle undergoing the reaction and ends on a gray block containing the resulting secondaries. As such, the first reaction in this event is inelastic scattering of a neutron by ^{72}Ge (not shown) resulting in a neutron, ^{72}Ge, and three gamma photons.

Figure 22. An event exhibiting photon production channel B in BGO exposed to a ^{252}Cf source.

In BGO exposed to a ^{239}Pu-Be neutron spectrum, 99.3% of total photon production was by scintillation and the remainder by Cerenkov radiation. We identified 612 unique production channels. As in the case of ^{252}Cf, 13 of these channels are responsible for a cumulative 91% of optical photon production as shown in Figure 23. Neutron inelastic scattering leading to Compton scattering and scintillation (Figure 24) produces 31% of optical photons, the same processes observed as channel B in ^{252}Cf (compare Figure 22 and Figure 24). The second leading channel produces 17% of optical photons through neutron inelastic scattering leading to the photoelectric effect and scintillation (Figure 25).

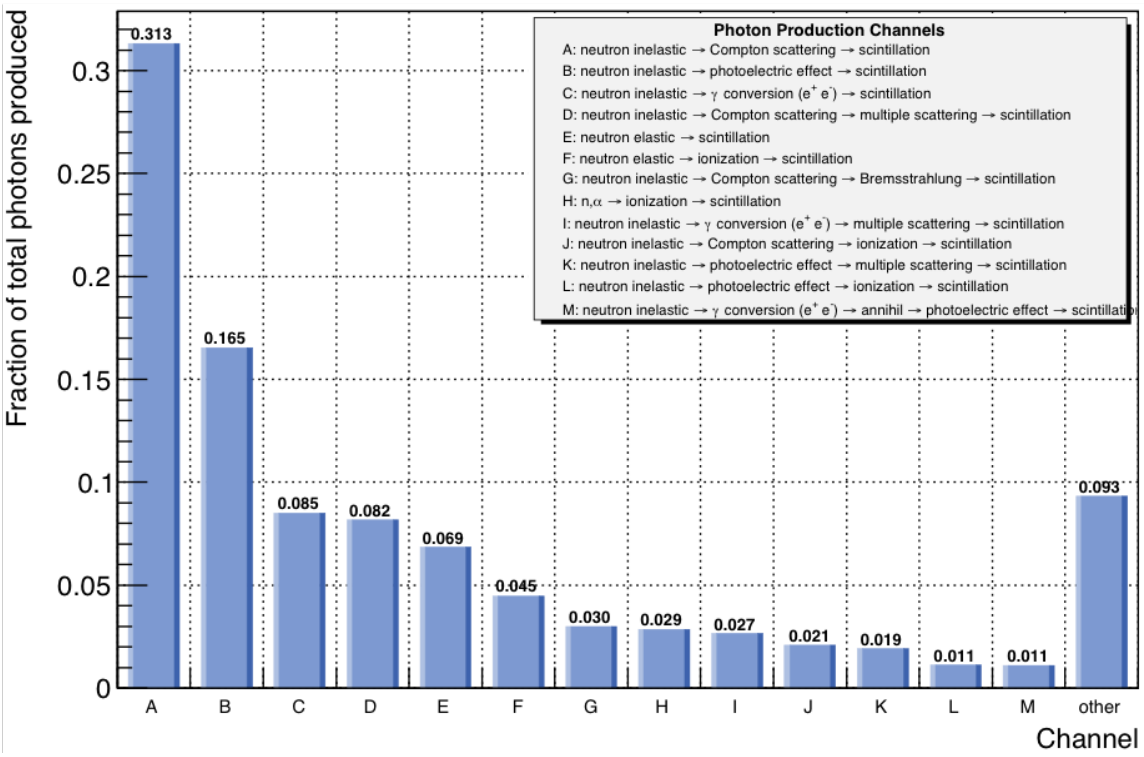

Figure 23. Photon production channels in simulated exposure of BGO to a ^{239}Pu-Be neutron spectrum

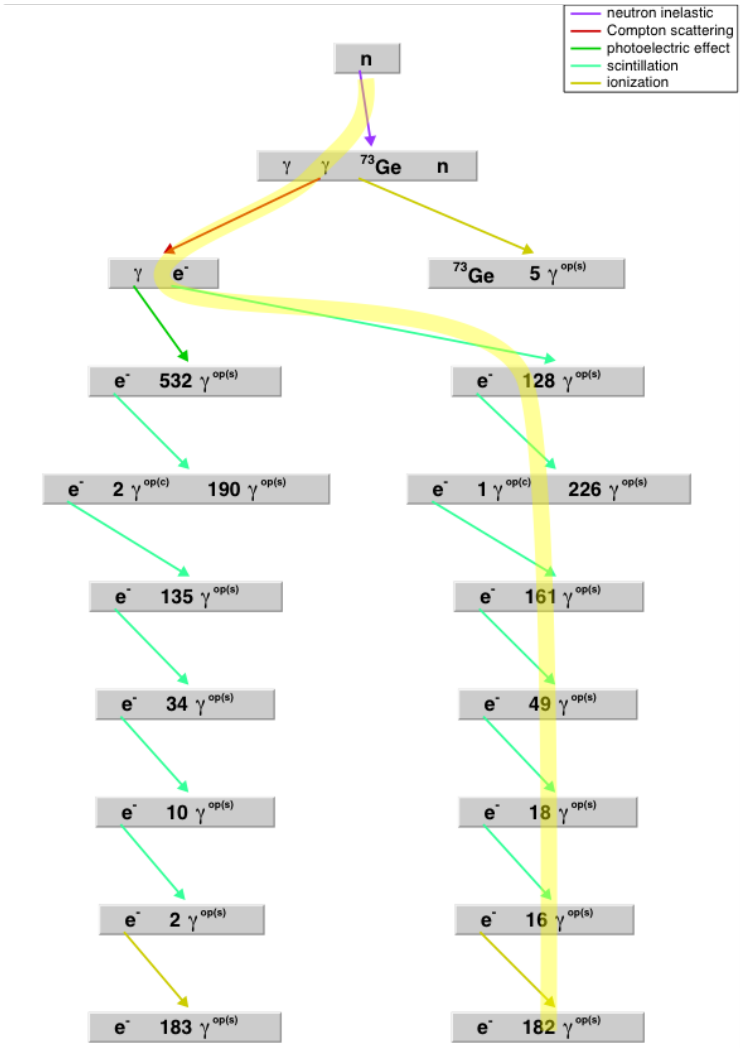

Photon production channel A (highlighted in yellow) is neutron inelastic scattering resulting in a gamma photon that undergoes Compton scattering. The resulting electron produces optical photons through scintillation. Note that channel B is also present in this event. Each arrow starts on the particle undergoing the reaction and ends on a gray block containing the resulting secondaries. As such, the first reaction in this event is inelastic scattering of a neutron by ^{73}Ge (not shown) resulting in a neutron, ^{73}Ge, and two gamma photons.

Figure 24. An event exhibiting photon production channel A in BGO exposed to a ^{239}Pu-Be source.

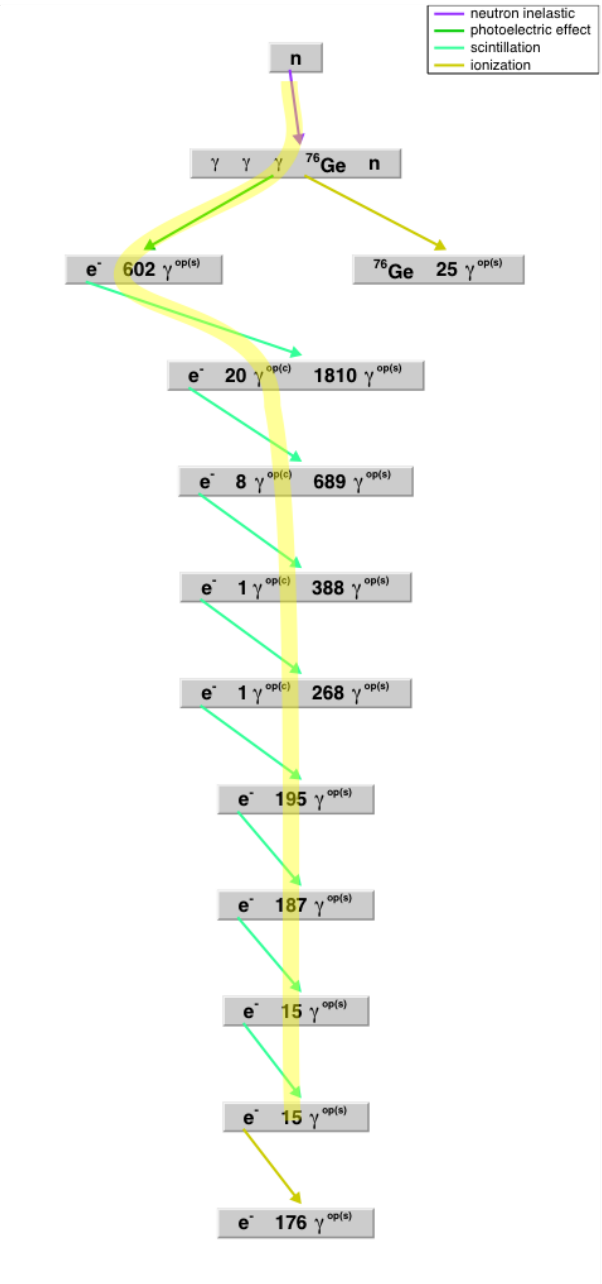

Photon production channel B (highlighted in yellow) is neutron inelastic scattering resulting in a gamma photon that, through the photoelectric effect, ejects an electron. The electron produces optical photons through scintillation. Note that channel L is also present in this event. Each arrow starts on the particle undergoing the reaction and ends on a gray block containing the resulting secondaries. As such, the first reaction in this event is inelastic scattering of a neutron by ^{76}Ge (not shown) resulting in a neutron, ^{76}Ge, and three gamma photons.

Figure 25. Photon production channel B in BGO exposed to a ^{239}Pu-Be source.

3. Photon Detection

In each simulation we recorded the energy of each optical photon reaching the photon detector. We observed that the energy spectrum of photons detected is very similar to that of photons produced. This similarity is expected since although the absorption coefficient of BGO does change with optical photon energy, the coefficient is an order of magnitude greater than the depth (i.e., cylindrical height) of the BGO target in our simulation. We also observed that, since the transport of optical photons is independent of the photon production channel, both the fraction of photons detected (73%) and the detected photon energy spectrum are similar for ^{252}Cf (Figure 26) and ^{239}Pu-Be (Figure 27) neutron spectra.

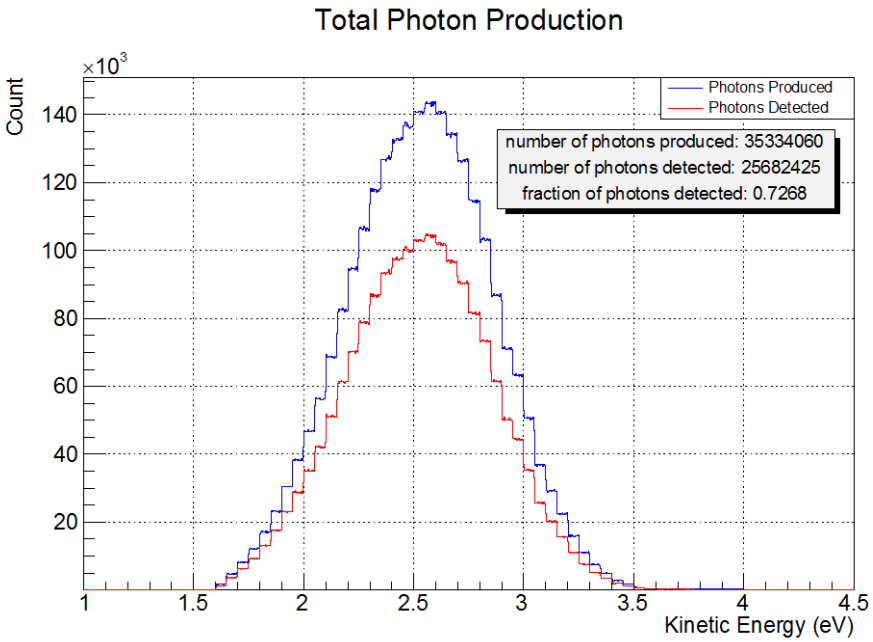

Figure 26. Optical photon production and detection in BGO simulated exposure to ^{252}Cf source

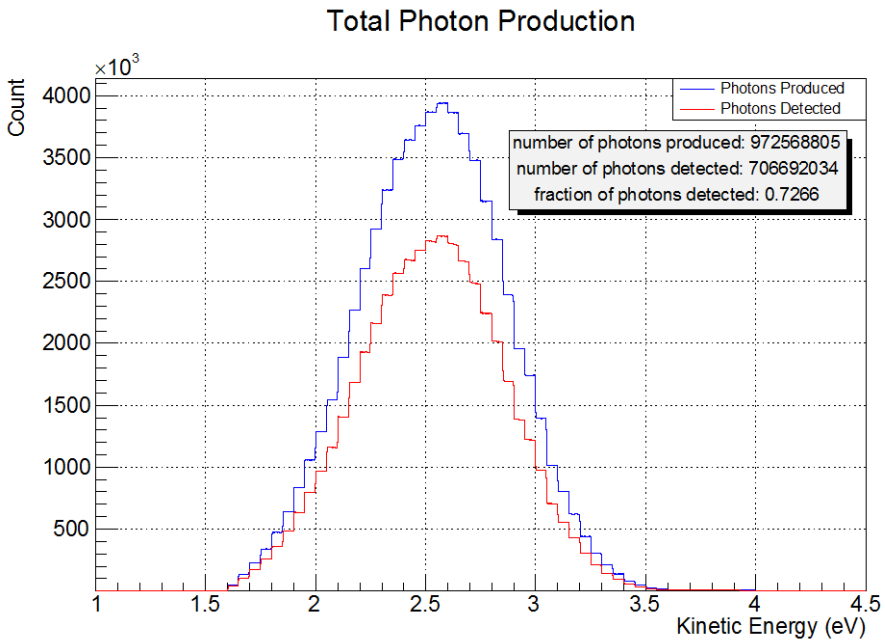

Figure 27. Optical photon production and detection in BGO simulated exposure to ^{239}Pu-Be source

C. CONCLUSION

We validated the simulation design by comparing the results to sets of independent known data. Based on these results, we selected LEND1.5.1 as the preferred physics list for this application. We confirmed the hypothesis of Ryzhikov et al. that elastic and inelastic neutron scattering are responsible for the majority of photon production, but observed that the exact contribution of each interaction depends strongly on the incident neutron energy spectra. Finally, we identified many photon production channels in BGO but observed that a small fraction of these channels account for over 90% of optical photons produced.

THIS PAGE INTENTIONALLY LEFT BLANK

V. CONCLUSION

This thesis has quantified the photon production channels from incident neutron to photon detection in BGO exposed to either ^{252}Cf or ^{239}Pu-Be neutron sources. This simulation provides a foundation for future work to model more complex detector geometries (e.g., ZEBRA detectors) with the intent of using modelling data to optimize heavy oxide scintillator detector design.

A. SUMMARY OF RESULTS

In this work, we evaluated four physics lists to be used in the simulation in conjunction with GEANT4, and we quantified the neutron interactions and the associated photon production channels in BGO exposed to two different neutron spectra.

1. Preferred GEANT4 Physics List

We evaluated three reference physics lists distributed with GEANT4 (FTFP_BERT_HP, Shielding, and ShieldingLEND) and one custom physics list developed at LLNL (LEND1.5.1). By comparing the simulation output using each physics list with three independent sets of known data, we conclude that although all four physics lists perform well, LEND1.5.1 and ShieldingLEND most closely reproduce experimental results. For the remainder of our work we implemented LEND1.5.1.

2. Quantification of the Neutron Interaction Channels in BGO

We observed that elastic and inelastic scattering of the incident neutrons yield over 90% of photon production in BGO, but the results vary significantly depending on the source neutron spectrum. In simulations of a ^{252}Cf neutron source, we observed that neutron elastic and inelastic scattering respectively yield 42.4% and 50.3% of the optical photons. In simulations of a ^{239}Pu-Be neutron source, the same reactions respectively yielded 11.9% and 82.7% of the optical photons.

Although neutron elastic and inelastic scattering dominate optical photon production, when normalized by the number of photons produced per neutron interaction,

we observe that neutron capture and *(n,p)* produce an order of magnitude more optical photons per interaction. We conclude that although elastic and inelastic scattering of neutrons produce relatively few neutrons per interaction, they dominate overall production because of the high cross sections of these interactions relative to other possible neutron interactions.

3. Evaluation of the Photon Production Channels in BGO

We defined a photon production channel as a unique sequence of interactions starting with a neutron interaction and ending in production of one or more optical photons. We identified 200 unique photon production channels in BGO exposed to a ^{252}Cf neutron source and 612 unique channels when exposed to a ^{239}Pu-Be neutron source. However, in each case, a single dominant channel accounted for almost one third of all optical photon production and the top 13 channels accounted for over 90%.

The dominant channel in ^{252}Cf was neutron elastic scattering followed by scintillation of optical photons. The dominant channel in ^{239}Pu-Be was neutron inelastic scattering resulting in a gamma photon that undergoes Compton scattering. The resulting electron produces optical photons through scintillation.

B. IMPLICATIONS

Although some experimental measurements were completed for both pure BGO and a BGO-based ZEBRA detector, the simulations in this work considered only pure BGO. In complex detector geometries such as ZEBRA detectors, it may be possible to use these simulation results to determine an optimal geometry that would maximize the neutron interactions and photon production channels we have identified. For instance, it may not be optimal for each layer in the ZEBRA detector to be identical. As the neutron loses energy traversing the detector and produces secondary particles, it may be possible optimize subsequent layers to increase the production of optical photons.

C. FUTURE RESEARCH

The object-oriented nature of GEANT4 lends itself to relatively straightforward evolution of the simulation. With an elementary understanding of C++, the detector target

can easily be changed to any material type or geometry provided the optical properties of the desired material are known. The neutron source can easily be changed to model different neutron spectra, to incorporate gamma spectra, or any number of other incident particles. The simulation data already collected can be further analyzed, the correlation with experimental results can be improved, and the simulation can evolve to model complex ZEBRA materials.

1. Further Analysis of Existing Data

A significant amount of simulation data has been collected and stored in ROOT TFiles. This data can be analyzed in many different ways using relatively simple Python scripts or ROOT macros. One possible area for additional analysis of the existing data is to consider which nuclei in BGO are involved in the various photon production channels.

2. Improved Correlation with Experimental Data

The comparison of the simulation with experimental results presented in Section IV.A.3 requires further work in order to draw a complete conclusion. The experimental setup for future work should incorporate detector shielding on all sides of the detector to prevent scattered gamma photons from contributing to the detected signal.

Additionally, the simulation did not account for the efficiency of the PMT, the PMT response function, and the preamplifier response function. Incorporating these features in the model would further improve the correlation with experimental data.

3. Modelling ZEBRA Materials

A natural next step in the evolution of this simulation is to model ZEBRA materials. The simulation of ZEBRA material is more complex than had initially been anticipated due to the random nature of the composite BGO-resin layers and the complexity of determining the optical properties of this proprietary mixture. Here, we suggest three possible ways to model this complex geometry.

a. Model the Composite Layer as a Homogenous Material

In order to implement this method, one would need to know the optical properties of the composite layer (not the individual properties of BGO and of the resin/binder). These optical properties would likely have to be determined experimentally due to the proprietary nature of the layer. Once the experimental data is determined, this would be simple to model; however, changing from BGO to another heavy oxide scintillator would require new experimental optical data.

b. Model the Composite Layer as Many Separate Volumes of BGO Embedded in a Volume of Binder Material

This would be very time consuming but not especially challenging to encode. Given the enormous number of logical volumes required, the simulation may not be stable and would likely be very slow to run. However, the optical properties of BGO are known and the optical properties of the binder/resin may be readily available. This implementation would be simple to change from BGO to another heavy oxide scintillator in future iterations.

c. Adapt NXSG4

NXSG4 is an extension to GEANT4 developed by Kittelmann and Boin at the European Spallation Source and is used for simulating polycrystalline or powdered crystalline materials [22]. Further analysis is required to determine if it is possible to adapt NXSG4 to model the ZEBRA composite layer. If possible, this would be the most flexible method of modelling ZEBRA materials as it would be simple to change from BGO to another heavy oxide scintillator in future iterations.

APPENDIX A. BGO MATERIAL DATA

Table 3. Spectral properties of BGO. Adapted from [23].

Photon Energy (eV)	Refractive Index	Absorption Coefficient (cm)	Scintillation Distribution
1.6	2.15	13.25	0
1.65	2.15	13	0.3
1.7	2.15	12.75	0.65
1.75	2.15	12.5	1.05
1.8	2.151	12.3	1.5
1.85	2.151	12.2	2.1
1.9	2.152	12	2.8
1.95	2.154	11.5	3.65
2	2.158	11.3	4.5
2.05	2.166	11.2	5.45
2.1	2.167	11	6.5
2.15	2.168	10.8	8.1
2.2	2.169	10.75	9.45
2.25	2.17	10.6	10.7
2.3	2.172	10.5	11.95
2.35	2.185	10.3	13.15
2.4	2.19	10.2	13.9
2.45	2.2	10.1	14.35
2.5	2.21	10	14.8
2.55	2.23	9.85	15.2
2.6	2.24	9.75	15.35
2.65	2.246	9.5	14.6
2.7	2.249	9.25	14.05
2.75	2.25	9	12.9
2.8	2.25	8.9	11.5
2.85	2.251	8.8	10.5
2.9	2.252	8.75	8
2.95	2.26	8.5	7.15
3	2.27	8.3	6.3
3.05	2.285	8.25	4.45
3.1	2.29	8.1	3.35
3.15	2.32	8.05	2.8
3.2	2.335	8	1.95
3.25	2.35	7.9	1.4
3.3	2.36	7.75	0.9
3.35	2.373	7.7	0.65
3.4	2.39	7.6	0.35
3.45	2.4	7.55	0.2
3.5	2.42	7.5	0.1
3.55	2.44	7.25	0.01
3.6	2.45	6.75	0
3.7	2.48	5.5	0
3.8	2.5	4	0
3.9	2.58	2.5	0
4	2.66	1	0

Table 4. Constant properties of BGO. Adapted from [8], [9], [24], and [25].

Optical Property	Value
Scintillation Yield	8.2 photons/keV [24]
Scintillation time constant	368.8 ns [8]
Bulk Modulus	102.8 GPa [25]
Isothermal Compressibility	1.556×10^{-24} m^3/MeV [a]
Yield Ratio	1 [b]
Resolution Scale	1 [c]

[a] Isothermal compressibility is the inverse of bulk modulus

[b] Yield ratio is the ratio of the fast and slow components of the scintillation yield. As BGO has only a fast component, the yield ratio is 1.

[c] Resolution scale is a measure of the spreading of photon energies about the specified scintillation yield. A value of 1 indicates a statistical distribution about the specified scintillation yield. [9]

APPENDIX B. NEUTRON SOURCE SPECTRA

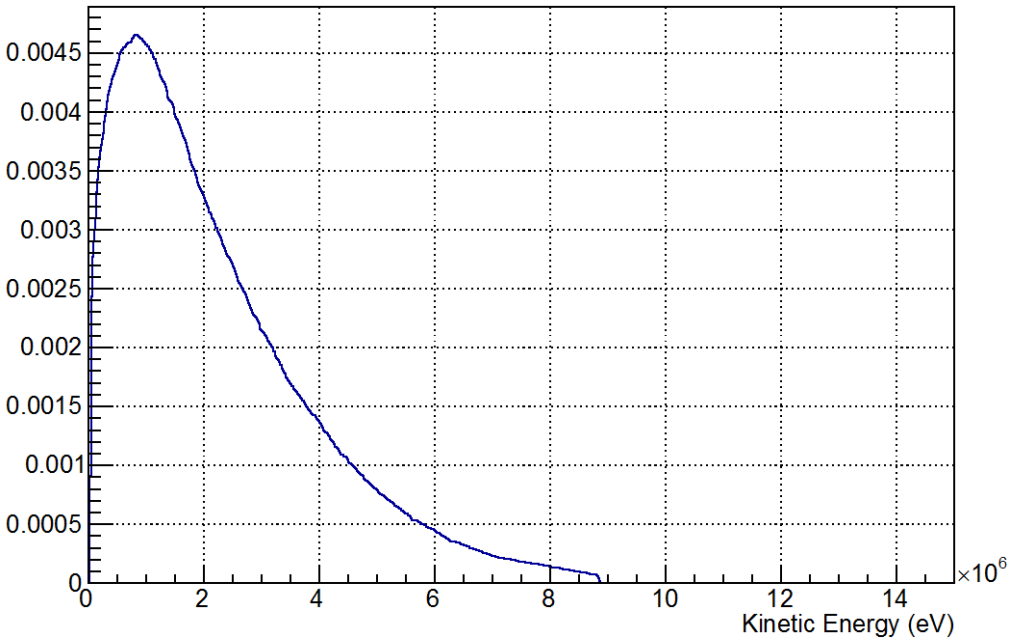

Figure 28. Normalized ^{252}Cf neutron spectrum used in simulation. Adapted from [26].

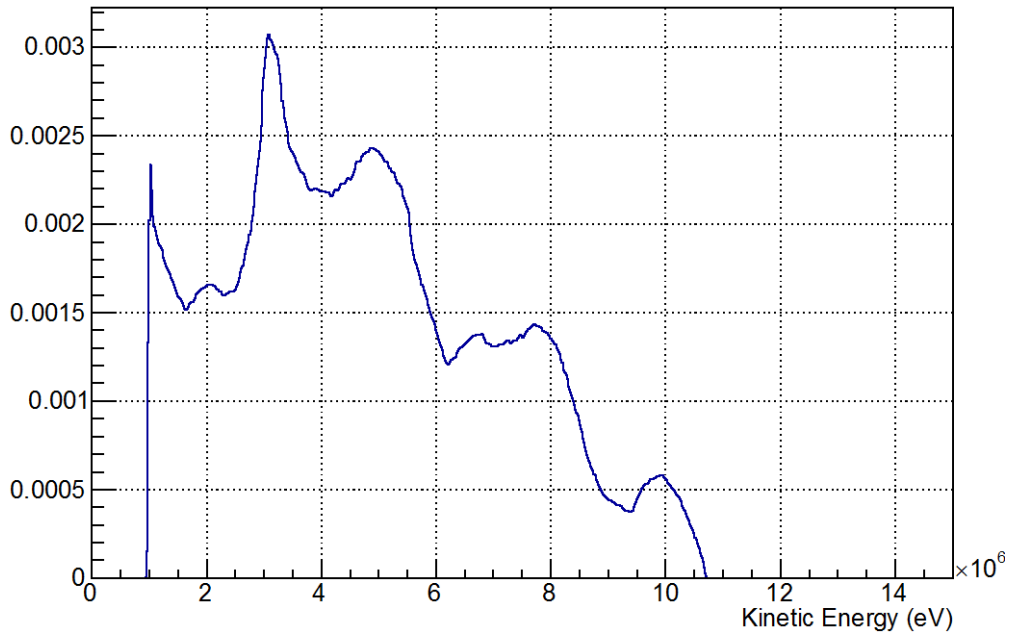

Figure 29. Normalized ^{239}Pu-Be neutron spectrum used in simulation. Adapted from [27].

THIS PAGE INTENTIONALLY LEFT BLANK

LIST OF REFERENCES

[1] V. D. Ryzhikov, S. V. Naydenov, G. M. Onyshchenko, L. A. Piven, T. Pochet, and C. F. Smith, “Multi-layer fast neutron detectors based on composite heavy-oxide scintillators for detection of illegal nuclear materials,” *Nucl. Instrum. Methods Phys. Res. Sect. Accel. Spectrometers Detect. Assoc. Equip.*, vol. 903, pp. 287–296, Sep. 2018.

[2] V. D. Ryzhikov, S. V. Naydenov, T. Pochet, G. M. Onyshchenko, L. A. Piven, and C. F. Smith, “Advanced multilayer composite heavy-oxide scintillator detectors for high-efficiency fast neutron detection,” *IEEE Trans. Nucl. Sci.*, vol. 65, no. 9, pp. 2547–2553, Sep. 2018.

[3] “ENDF: Evaluated Nuclear Data File.” Accessed January 15, 2019. [Online]. Available: https://www-nds.iaea.org/exfor/endf.htm

[4] V. D. Ryzhikov and Institute for Scintillation Materials, STC “Institute for Single Crystals,” National Academy of Science of Ukraine, 60 Nauky Ave., 61072 Kharkiv, Ukraine, “Multi-layered composite detectors for neutron detection,” *Funct. Mater.*, vol. 25, no. 1, pp. 172–179, Mar. 2018.

[5] J. Allison *et al.*, “Recent developments in Geant 4,” *Nucl. Instrum. Methods Phys. Res. Sect. Accel. Spectrometers Detect. Assoc. Equip.*, vol. 835, pp. 186–225, Nov. 2016.

[6] R. Brun and F. Rademakers, “ROOT—An object oriented data analysis framework,” *Nucl. Instrum. Methods Phys. Res. Sect. Accel. Spectrometers Detect. Assoc. Equip.*, vol. 389, no. 1–2, pp. 81–86, Apr. 1997.

[7] J. B. Birks, *The Theory and Practice of Scintillation Counting*. New York: Pergamon Press, 1964.

[8] S. I. Ziegler, J. G. Rogers, V. Selivanov, and I. Sinitzin, “Characteristics of the new YAlOCe compared with BGO and GSO,” *IEEE Trans. Nucl. Sci.*, vol. 40, no. 2, pp. 194–197, Apr. 1993.

[9] “Book For Application Developers 10.5 documentation.” Accessed January 31, 2019. [Online]. Available: http://geant4-userdoc.web.cern.ch/geant4-userdoc/UsersGuides/ForApplicationDeveloper/html/Detector/material.html

[10] W. J. Price, *Nuclear Radiation Detection*, 2nd ed. New York: McGraw-Hill Book Company, 1958.

[11] P. A. Williams, A. H. Rose, K. S. Lee, D. C. Conrad, G. W. Day, and P. D. Hale, "Optical, thermo-optic, electro-optic, and photoelastic properties of bismuth germanate $Bi_4Ge_3O_{12}$," *Appl. Optics*, vol. 35, no. 19, pp. 3562–3569, 1996. [Online]. https://doi.org/10.1364/AO.35.003562

[12] S. Agostinelli *et al.*, "Geant4—a simulation toolkit," *Nucl. Instrum. Methods Phys. Res. Sect. Accel. Spectrometers Detect. Assoc. Equip.*, vol. 506, no. 3, pp. 250–303, Jul. 2003.

[13] J. T. Goorley *et al.*, "Initial MCNP6 release overview—MCNP6 version 1.0," LA-UR-13-22934, 1086758, Jun. 2013.

[14] T. Goorley *et al.* (2012) "Initial MCNP6 release overview," *Nuclear Technol.*,vol. 180, no, 3, pp. 298–315. [Online]. doi: 10.13182/NT11-135

[15] "Geant4 physics reference manual—physics reference manual 10.5 documentation." [Online]. Available: http://geant4-userdoc.web.cern.ch/geant4-userdoc/UsersGuides/PhysicsReferenceManual/html/index.html. [Accessed: 10-Apr-2019].

[16] J. M. Verbeke, "HPNeutron vs LEND," 14-Feb-2019.

[17] *Geant4*. Geant4 Collaboration, Geneva. 2019. Available https://geant4.web.cern.ch.

[18] C. Domingo-Pardo *et al.*, "New measurement of neutron capture resonances in ^{209}Bi," *Phys. Rev. C*, vol. 74, no. 2, Aug. 2006.

[19] K. S. Krane and D. Halliday, *Introductory Nuclear Physics*. New York: Wiley, 1987.

[20] J. R. Taylor, *An Introduction to Error Analysis: The Study of Uncertainties in Physical Measurements*, 2nd ed. Sausalito, CA: University Science Books, 1997.

[21] J. M. Verbeke, "Pulse Shaping," 25-Jul-2019.

[22] T. Kittelmann and M. Boin, "Polycrystalline neutron scattering for Geant4: NXSG4," *Comput. Phys. Commun.*, vol. 189, pp. 114–118, 2015.

[23] H. Wenzel, "Simulation of total absorption dual readout calorimetry." Fermilab, 02-Aug-2010.

[24] I. Holl, E. Lorenz, and G. Mageras, "A measurement of the light yield of common inorganic scintillators," *IEEE Trans. Nucl. Sci.*, vol. 35, no. 1, pp. 105–109, Feb. 1988.

[25] M. Lebeau, “Monocrystalline bismuth germanate $Bi_4Ge_3O_{12}$ (BGO) recent results on mechanical properties,” *J. Mater. Sci. Lett.*, vol. 4, pp. 779–782, 1985.

[26] A. B. Smith, P. R. Fields, and J. H. Roberts, “Spontaneous fission neutron spectrum of ^{252}Cf,” *Phys. Rev.*, vol. 108, no. 2, pp. 411–413, Oct. 1957.

[27] A. Kumar and P. S. Nagarajan, “Neutron spectra of ^{239}Pu-Be neutron sources,” *Nucl. Instrum. Methods*, vol. 140, no. 1, pp. 175–179, 1977.

THIS PAGE INTENTIONALLY LEFT BLANK

INITIAL DISTRIBUTION LIST

1. Defense Technical Information Center
   Ft. Belvoir, Virginia

2. Dudley Knox Library
   Naval Postgraduate School
   Monterey, California